Asymmetric response of the subtropical western South Atlantic thermocline to the Dansgaard-Oeschger events of Marine Isotope Stages 5 and 3

Thiago P. Santos [a, *], João M. Ballalai [a], Daniel R. Franco [b], Rômulo R. Oliveira [b], Douglas O. Lessa [a], Igor M. Venancio [c], Cristiano M. Chiessi [d], Henning Kuhnert [e], Heather Johnstone [e], Ana Luiza S. Albuquerque [a]

[a] *Programa de Geociências (Geoquímica), Universidade Federal Fluminense, Niterói, Brazil*
[b] *Coordenação de Geofísica, Observatório Nacional, Rio de Janeiro, Brazil*
[c] *Center for Weather Forecasting and Climate Studies (CPTEC), National Institute for Space Research (INPE), Cachoeira Paulista, Brazil*
[d] *Escola de Artes, Ciências e Humanidades, Universidade de São Paulo, São Paulo, Brazil*
[e] *MARUM-Center for Marine Environmental Sciences, University of Bremen, Bremen, Germany*

A R T I C L E   I N F O

A B S T R A C T

The last glacial period (116−11.7 ka BP) was an interval characterized by a sequence of abrupt millennial-scale events well documented in Greenland and Antarctica ice-cores. Throughout this period, Greenland cold stadials were accompanied by warm conditions in the thermocline to intermediate waters of the Atlantic Ocean that may have played a role in both the basal melting of ice shelves and the rapid atmospheric warming during the onset of warm interstadials. Climate model simulations indicated an accentuated response of the subtropical western South Atlantic thermocline to the disturbances in the Atlantic circulation. Such works encourage investigations upon thermocline/deep-dwelling planktic foraminifera in this region; however, a study with this aim was not performed. Here we present a paleoceanographic reconstruction from the subtropical western South Atlantic based on the thermocline planktic foraminifera *Globorotalia inflata*. Our high-resolution δ^{18}O record for the last glacial period presents a millennial-scale variability that strongly resembles the structure of the Greenland Dansgaard-Oeschger cycles during Marine Isotope Stage (MIS) 5. During MIS 3, this millennial-scale variability is absent or considerably dampened. Mg/Ca-derived temperature and seawater δ^{18}O corrected for ice-volume for the MIS 5 interval demonstrate that the region was warmer and saltier (colder and fresher) during early-glacial stadials (interstadials). Our data suggest a reorganization of the northward heat transport throughout the last glacial, in which regions as far south as 24 °S acted as heat reservoirs in periods of weakened Atlantic Meridional Overturning Circulation during MIS 5 but not necessarily (or only marginally) during MIS 3.

© 2020 Elsevier Ltd. All rights reserved.

1. Introduction

Paleoclimatic records, mainly those recovered in the northern hemisphere (e.g., Voelker, 2002), reveal that the last glacial period, the interval between 116 and 11.7 ka BP, was marked by a series of abrupt and recurrent climatic oscillations (Elliot et al., 2002; Genty et al., 2003; EPICA Community Members, 2004; NGRIP Community Members, 2004; Skinner and Elderfield, 2007; Wang et al., 2008; Deplazes et al., 2013). Known as Dansgaard-Oeschger (DO) cycles, these centennial-to millennial-scale oscillations are associated with warm or cold conditions around Greenland, that showed dramatic air temperature shifts by more than 10 °C (Blunier and Brook, 2001; Steig and Alley, 2002; Lohmann and Ditlevsen, 2018). Despite their high relevance, uncertainties remain regarding the causes of DO cycles. Existing hypotheses include forcing by a dipole in salt accumulation between low and high latitudes of the Atlantic Ocean, the stochastic resonance of the glacial climate caused by ice-sheet dynamics, the impact of ocean

temperature over the ice-shelf width and basal melting, brine rejection in the Nordic Seas, changes in the height of the Northern Hemisphere ice-sheet, changes in insolation and volcanic activity (e.g., Sakai and Peltier, 1999; Alley et al., 2001; Bay et al., 2004; Braun et al., 2008; Alvarez-Solas et al., 2010; Dokken et al., 2013; Zhang et al., 2014).

It is generally accepted that DO cycles were accompanied by fluctuations in the intensity of the Atlantic Meridional Overturning Circulation (AMOC), which moved from a vigorous mode during Greenland interstadials (GI − the warm phase of DO cycles) to a weak mode during Greenland stadials (GS − the cold phase of DO cycles) (Broecker et al., 1988; Seidov and Maslin, 2001; Hagen and Keigwin, 2002; Gottschalk et al., 2015; Henry et al., 2016). As the AMOC southward deep return flow is colder and fresher than the near-surface northward flow, these millennial-scale abrupt events typify some of the most significant natural reorganizations in the Atlantic Ocean heat and salt transport (Chapman and Shackleton, 1998; Knorr and Lohmann, 2003; Rühlemann et al., 2004). In the current scenario, in which an AMOC weakening until the end of the century and beyond is very likely (e.g., Liu et al., 2017; Caesar et al., 2018), DO cycles may be used to illustrate the concept of AMOC bistability that operate during intervals of climate system disequilibrium (Rahmstorf et al., 2005; Ditlevsen and Johnsen, 2010). The AMOC variability synchronous to the DO cycles resulted in opposite temperature fields between northern and southern latitudes (e.g., Zarriess et al., 2011; WAIS Divide Project Members et al., 2015) − a condition commonly referred as a thermal bipolar seesaw and that was established from Crowley (1992) and Stocker and Johnsen (2003) studies. In the thermal bipolar seesaw, the Southern Ocean would work as a heat reservoir that gradually accumulates energy when northward heat transport declines under a weak AMOC (Stocker and Johnsen, 2003). According to Buizert and Schmittner (2015), the AMOC stability and timing of the DO oscillations are linked to the Southern Hemisphere climate via processes like the wind-driven upwelling of North Atlantic Deep Water (NADW) in the Southern Ocean. A southward positioning of the southern westerlies would pump NADW to the upper Southern Ocean and consequently increase the deep-water convection in the northern Atlantic, maintaining the AMOC strength. When overall Antarctic temperatures are high, and westerlies are likely in a southernmost position, such as during Marine Isotope Stage (MIS) 5, GI tends to last longer ($>10^3$ yr) due to the stability of the NADW wind-driven upwelling. By contrast, during Antarctic cold periods, like MIS 4 and 2, GI tends to be shorter ($<10^3$ yr) or completely absent (Buizert and Schmittner, 2015). Southern Ocean warming would make the AMOC less susceptible to disturbances (like freshwater discharge in the northern Atlantic) and raises the threshold for an AMOC shutdown (Buizert and Schmittner, 2015). Hence, it is reasonable to hypothesize that the warmer climate of MIS 5 compared with MIS 3 would require more powerful disturbances to slowdown the AMOC and the consequences (e.g., Atlantic inter-hemispheric temperature gradients) would also be more prominent.

A recent re-evaluation of the thermal bipolar seesaw hypothesis through transient simulations challenges the often assumed role of the Southern Ocean as the primary heat reservoir (Pedro et al., 2018). This work showed that the Southern Ocean heat reservoir alone is not able to account for the fast inter-hemispheric coupling required to explain the modeling results and the observations. The global thermocline/intermediate ocean to the north of the Antarctic Circumpolar Current, in turn, would act much more efficiently to store heat during a GS and the concurrent AMOC slowdown (Rühlemann et al., 2004; Pedro et al., 2018). This is the case of the western South Atlantic, which presents one of the most substantial thermal response to the DO disturbance at thermocline levels in

model simulations (Schmittner et al., 2003; Pedro et al., 2018). Idealized experiments also investigated the timing and directionality of the abrupt signal through the Atlantic (e.g., Peltier and Vettoretti, 2014). The simulations tend to indicate a north-to-south transmission with an almost synchronous response of the South Atlantic thermocline to the imposed changes in the northern high-latitude convection. Deep-dwelling species of planktic foraminifera have the potential to record changes in temperature and salinity at thermocline levels in the subtropical western South Atlantic (Chiessi et al., 2007; Cléroux et al., 2008), but direct observations from this region are lacking.

Here we present new downcore records of thermocline stable oxygen isotopes (δ^{18}O), Mg/Ca-derived temperatures, and seawater δ^{18}O corrected for ice volume ($\delta^{18}O_{IVF-SW}$) from the subtropical western South Atlantic (Brazil margin − Santos Basin; core GL-1090) based on analyses of thermocline-dweller planktic foraminifera *Globorotalia inflata*. We also performed a cross-correlation analysis between our thermocline δ^{18}O and northern and southern ice-core δ^{18}O in order to distinguish the potential sources of millennial-scale instabilities and signal propagation to the studied area. Our high-resolution thermocline δ^{18}O data shows distinct millennial-scale variability during MIS 5 that strongly resembles the structure of DO cycles. On the other hand, during MIS 3, this DO-like pattern is eventually absent (early-MIS 3) or weakly represented (mid-to late-MIS 3). Reduced DO variability in the subtropical western South Atlantic during MIS 3 may suggest that the northward transfer of energy from latitudes as far south as 24 °S was not as persistent/dominant as during MIS 5. Therefore, our results allow testing the southern extent of thermocline response to North Atlantic abrupt climate events to a level that was previously not possible.

2. Material and methods

2.1. Study area

We analyzed marine sediment core GL-1090 (24.92 °S, 42.51 °W, 2225 m water depth, 1914 cm long) that was collected by the Petrobras oil company in the subtropical western South Atlantic (Santos Basin, Fig. 1). The uppermost circulation (0−600 m) in the area is dominated by the southward-flowing Brazil Current (Stramma and England, 1999). Due to the high incoming solar radiation and excess evaporation that characterize the tropical South Atlantic (ca. 10 °S) in the region where the Brazil Current is formed, the Brazil Current at the surface is composed of warm (>20 °C) and saline (>36) Tropical Water. Around 38 °S, the Brazil Current collides with the northward-flowing Malvinas Current, producing the Brazil−Malvinas Confluence, where most of the South Atlantic Central Water (SACW) is formed (Garzoli and Matano, 2011) through air-sea interactions. SACW is also produced in the areas adjacent to the Argentine basin and mid-Atlantic ridge along the South Atlantic Current (Garzoli and Matano, 2011). SACW is colder (6−20 °C) and fresher (>34.6−36) than Tropical Water, and it ventilates the South Atlantic thermocline incorporated into the subtropical gyre. Along the Brazilian margin, SACW is transported southwards by the Brazil Current below the Tropical Water. In addition to the differences in their temperatures and salinities, Tropical Water and SACW can also be distinguished by the δ^{13}C values of their dissolved inorganic carbon, as the $\delta^{13}C_{DIC}$ in the Tropical Water is 1.74 ± 0.24‰ while that in the SACW is 1.30 ± 0.22‰ (Venancio et al., 2014). This offset is due to the higher nutrient content in the central waters, as the $\delta^{13}C_{DIC}$ decreases with increasing nutrient concentration (Kroopnick, 1985). SACW is also sourced from Indian Ocean Central Water and brought into the South Atlantic by Agulhas eddies in the upper 1000 m of the water
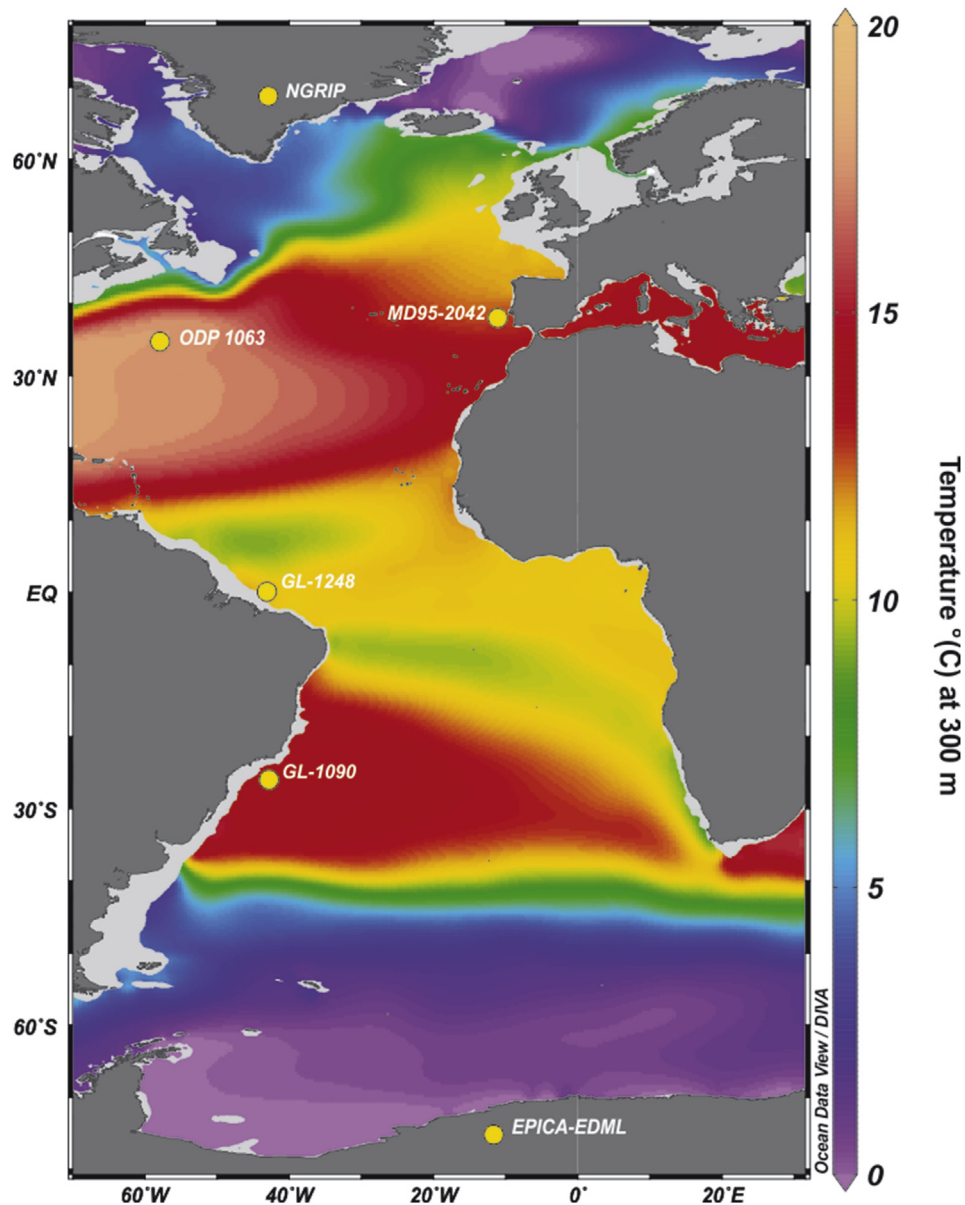
Fig. 1. Position of core GL-1090 (this study) and other marine and ice-core records discussed in this work. GL-1248 (2264 m) (Venancio et al., 2018), ODP Site 1063 (4584 m) (Thornalley et al., 2013), MD95-2042 (3146 m) (Shackleton et al., 2000; =Govin et al., 2014a), NGRIP (NGRIP Community Members, 2004) and EPICA-EDML (EPICA/EDML Community Member, 2004). The temperature grid refers to the 300 m depth (Locarnini et al., 2013). The figure was produced using the software Ocean Data View (Schlitzer, 2017).

column (Richardson, 2007). Tropical Water and SACW are the main water masses influencing the upper ocean at the GL-1090 site, and their geochemical properties are recorded by surface and deep-dwelling planktic foraminifera species, respectively.

2.2. GL-1090 age model

The chronology of the 1914 cm of core GL-1090 (2225 m water depth; Santos et al., 2017a) was obtained through the combination of calibrated AMS ^{14}C ages and benthic foraminifera δ^{18}O tie-points aligned to two reference curves (Lisiecki and Raymo, 2005; Govin et al., 2014). We focused on the interval of the last interglacial-glacial cycle, which refers to the upper 1365 cm of core GL-1090. As the discussion presented here relies heavily on the comparison of planktic foraminifera δ^{18}O with Greenland millennial-scale events, we implemented changes in the previously published

(Santos et al., 2017a) age model on the referred interval to improve the correspondence of our record to the NGRIP ice-core on the AICC2012 time-scale (Bazin et al., 2013; Veres et al., 2013). As explained in Santos et al. (2017a), the AMS ^{14}C ages were calibrated with the curve Marine13 (Reimer et al., 2013), applying a regional ΔR of 7 ± 59 (Angulo et al., 2007). A ^{14}C age reversal was identified at 327 cm and excluded from the final age-depth modeling. We kept the tuning between the *Cibicides wuellerstorfi* δ^{18}O of GL-1090 and benthic of δ^{18}O MD95-2042 (which has its age model based on the alignment between *Globigerina bulloides* δ^{18}O and NGRIP on the Antarctic Ice Core Chronology (AICC2012) time-scale (Veres et al., 2013; Govin et al., 2014) (Fig. 2A). GL-1090 and MD95-2042 (3146 m water depth) are influenced by upper and lower portions of the same water mass (NADW), respectively. Further, the benthic δ^{18}O of MD95-2042 offers the possibility to align millennial-scale events present in the benthic δ^{18}O of GL-1090 in this portion,

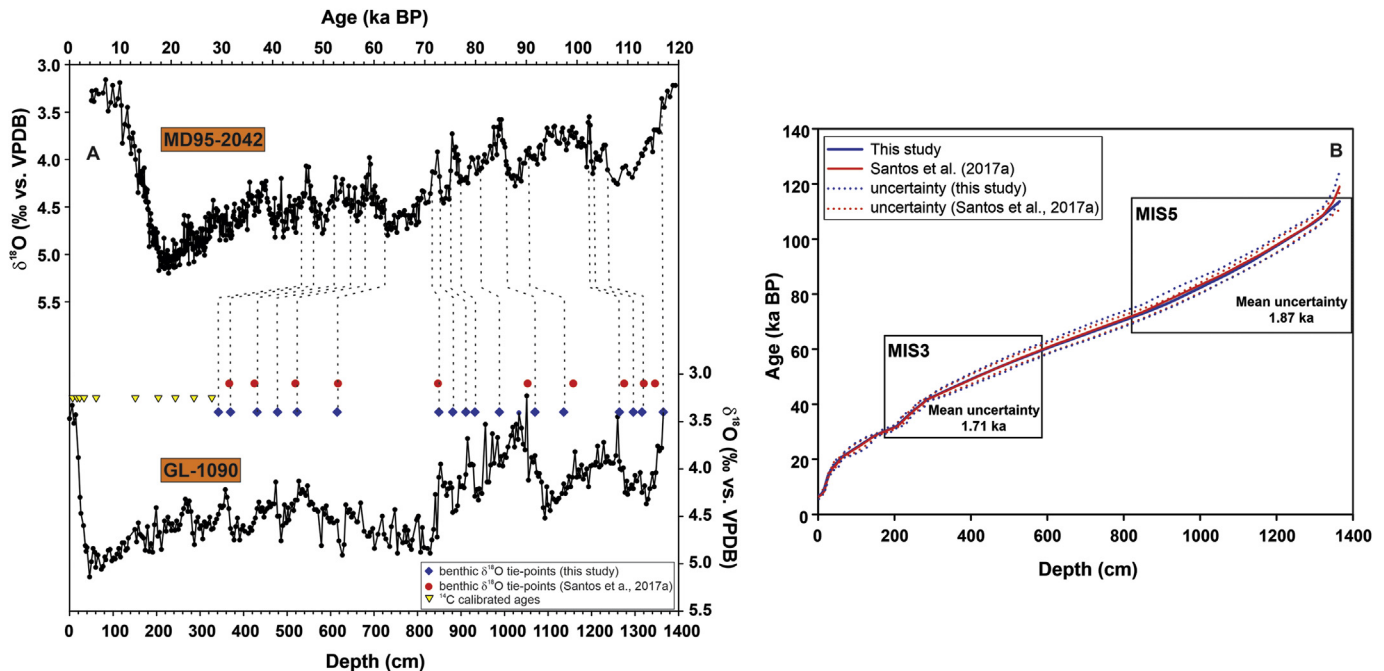**Fig. 2.** A: Alignment between benthic δ^{18}O of MD95-2042 (upper panel) on the AICC2012 time-scale (Bazin et al., 2013; Veres et al., 2013; Govin et al., 2014) and benthic δ^{18}O of GL-1090 (lower panel). Blue diamonds and red circles on the lower panel denote the position of revised (this study) and earlier benthic δ^{18}O tie-points (Santos et al., 2017a), respectively. Yellow triangles indicate the calibrated ^{14}C age. B: Bayesian age-depth model of core GL-1090 developed within software Bacon v. 2.3 (Blaauw and Christeny, 2011). Thick and dashed blue (this study) and red (Santos et al., 2017a) lines indicate the modeled age and associated uncertainty, respectively. (For interpretation of the references to colour in this figure legend, the reader is referred to the Web version of this article.)

which is not the case of LR04 (Lisiecki and Raymo, 2005) (Fig. 2A). In this first 1365 cm, we increased the number of the visually determined benthic δ^{18}O tie-points, so that, a chronological control existed at the onset and demise of each millennial-scale event presented in the benthic δ^{18}O of GL-1090. Error estimation of δ^{18}O tie-points determination take into account the mean resolution of the GL-1090 benthic δ^{18}O record around the tie-point depth, the mean resolution of the reference curve around the tie-point age, a matching error visually estimated when defining the tie-points, and the absolute age error of the time-scale used for the reference record (Santos et al., 2017a). The age control points are provided in Table 1. The mean sampling resolution for the proxies developed here was ca. 0.2 ka and 0.3 ka for the *G. inflata* δ^{18}O and for the Mg/Ca-derived temperature and δ^{18}O$_{IVF-SW}$, respectively.

The complete age-depth model was built within the software Bacon v. 2.3, which uses Bayesian statistics to reconstruct Bayesian accumulation histories for sedimentary deposits (Blaauw and Christeny, 2011). The rise in the number of tie-points was beneficial for the GL-1090 age model since the increase in dating density improves the precision of Bayesian age-depth models (Blaauw et al., 2018). The reassessment executed here did not change significantly earlier sedimentation rates estimated for core GL-1090 and, in most of the parts, the ages and their minimum and maximum uncertainty envelopes overlapped (Fig. 2B). Mean age uncertainty (2σ) estimated with Bacon around the interstadials chosen as tie-points for MIS 5 and 3 are 1.87 and 1.71 ka, respectively (Table 1 and Fig. 2B). Bacon was employed with default parameters together with ten thousand age-depth runs to estimate mean age and 95% confidence interval at the desired resolution for each proxy. As shown in Mulitza et al. (2017), for the proxies presented in this study, ten thousand series were estimated by mixing the age-depth previously estimated by Bacon with ten thousand downcore Monte Carlo proxy realization within the analytical uncertainty. This procedure determines the confidence intervals in

the 95% uncertainty envelope for each proxy at the mean ages of the individual sample depths (Mulitza et al., 2017).

2.3. Geochemical analyses on the planktic foraminifera Globorotalia inflata

δ^{18}O of deep-dweller *G. inflata* (with apparent calcification depth of ca. 400 m in the subtropical western South Atlantic; Chiessi et al., 2007) was initially explored for the transitions between MIS 6/5e and MIS 2/1 (Santos et al., 2017b). In this study, we present new *G. inflata* δ^{18}O data that, together with the previously published data, cover the entire last interglacial-glacial cycle (upper 1365 cm of core GL-1090), which consists of 542 samples. For every sample, between 5 and 10 shells of *G. inflata* from the 250−300 μm size fraction were handpicked under a stereomicroscope. Stable isotope analyses were performed at the MARUM-Center for Marine Environmental Sciences, University of Bremen, Germany, using a Finnigan MAT252 isotope ratio mass spectrometer attached to a Kiel III automated carbonate preparation device. Data were calibrated against an in-house standard (Solnhofen limestone). The results are reported in per mil (‰, parts per thousand) versus Vienna Peedee belemnite (VPDB). The standard deviation based on replicate measurements of the in-house standard was 0.06‰.

G. inflata Mg/Ca-derived temperature was initially explored for the transition between MIS 6/5e (Ballalai et al., 2019). In this study, we extend the *G. inflata* Mg/Ca data to cover the period between the onset of the last glacial until the mid-MIS 4 (from 1365 to 699 cm of core GL-1090) in which 183 samples were analyzed. Cleaning procedures followed precisely those reported in Ballalai et al. (2019), which were based on the protocol of Barker et al. (2003). The diluted solutions were analyzed with an Inductively Coupled Plasma Optical Emission Spectrometer (ICP-OES)—Agilent Technologies 700 Series with Cetac ASX-520 autosampler and a micronebulizer at the MARUM − Center for Marine Environmental

Table 1
The AMS[14]C ages and Cibicides wuellerstorfi δ^{18}O tie-points of core GL-1090 tuned to the age model of MD95-2042 on the AICC2012 time-scale (Veres et al., 2013; Govin et al., 2014). For the case of AMS[14]C dates, the age in centimeter 327 (BETA-404142) was considered as a reversal, and it was not included in the age-depth modeling within the software Bacon v.2.3. For the case of benthic δ^{18}O, linear estimated ages (ka BP) refers to the age determined during the visual tuning process. Bacon final calendar ages (ka BP) refer to the ages built after the Bayesian age-depth modeling.

Laboratory code	Depth (cm)	AMS[14]C Age (ka)	Bacon calibrated[14]C age (ka BP)	Mean Bacon estimated uncertainty (ka)
BETA-404133	7	6.69	7.23	0.05
BETA-404134	17	9.12	9.87	0.10
BETA-404135	23	11.35	12.80	0.08
BETA-404136	33	13.76	16.03	0.10
BETA-404137	61	17.58	20.68	0.15
BETA-404138	151	25.26	28.80	0.20
BETA-404139	204	28.36	31.91	0.25
BETA-404140	243	33.29	36.89	0.66
BETA-404141	286	37.93	41.73	0.45
BETA-404142	327	37.69	44.41	0.49
Benthic δ^{18}O tie-point position	**Depth (cm)**	**Linear estimated age (ka BP)**	**Bacon final calendar age (ka BP)**	**Mean Bacon estimated uncertainty (ka)**
End of GI-12	342	45.80	45.37	1.41
Onset of GI-12	370	47.80	47.15	1.58
End of GI-14	431	52.10	50.92	1.76
Onset of GI-14	478	55.30	53.71	1.81
End of GI-16/17	523	58.50	56.23	1.86
Onset of GI-16/17	615	62.10	61.14	1.86
End of GI-19	849	71.50	72.92	1.70
Onset of GI-19	881	73.10	74.65	1.62
End of GI-20	911	75.10	76.40	1.60
Onset of GI-20	932	76.80	77.72	1.62
End of GI-21	988	81.20	81.48	1.77
Onset of GI-21	1070	86.10	87.12	1.94
End of GI-23	1136	90.30	92.21	2.08
Onset of GI-23	1264	102.80	102.99	2.10
End of GI-24	1296	103.70	105.78	2.10
Onset of GI-24	1316	106	107.80	2.25
Transition to last glacial inception	1365	116.70	113.64	3.06

Sciences, University of Bremen, Germany. Three replicates of each sample were run and averaged. Elements were measured at the following spectral lines: Mg (279.6 nm), Ca (315.9 nm), Sr (421.6), Al (167.0 nm), Fe (238.2 nm), and Mn (257.6 nm). Calibration standards consisted of dissolution acid (0.075 M HNO_3) as blank and four multielement standards between 20 and 80 ppm Ca, with Mg/Ca of 4.12 mmol/mol. Calibrations for all elements were based on linear regressions. Instrumental precision was monitored by using an in-house standard solution, run after every five samples. The long-term relative standard deviation of the in-house standard is <2% for Mg/Ca. A dissolved solution of commercial limestone standard ECRM 752-1 was measured every 30 samples as an external standard. This solution was measured at 3.73 mmol/mol ($\sigma = 0.01$, 0.24%, n = 9) during the ICP-OES run, which is very close to the published value of 3.75 mmol/mol for a centrifuged solution (Greaves et al., 2005). Eleven samples (ca. 6% of the total) had <10 ppm Ca and were rejected, as the calibration is non-linear at low Ca concentrations. The Al/Ca, Fe/Ca, and Mn/Ca ratios were analyzed to monitor the efficiency of the cleaning. The samples showed averages of 0.30, 0.46, and 0.55 mmol/mol of Al/Ca, Fe/Ca, and Mn/Ca, respectively. The Al/Ca ratio falls close to the commonly accepted limits of 0.30–0.50 mmol/mol (Lea et al., 2005; Kuhnert et al., 2014) and had no correlation with Mg/Ca ($R^2 = 0.018$) (Supporting Fig. 1). The Fe/Ca and Mn/Ca ratios were higher than the 0.1 mmol/mol cut off proposed by Barker et al. (2003). However, the lack of correlation between our Mg/Ca ratio and both the Fe/Ca ($R^2 = 0.001$) and Mn/Ca ($R^2 = 0.0001$) ratios suggests that our analyses were not significantly affected by Fe–Mn-oxyhydroxides (Supporting Fig. 1). Other studies also found values for Fe/Ca and Mn/Ca ratios that were higher than those given by Barker et al. (2003) (e.g., Lea et al., 2005; Weldeab et al., 2006; Groeneveld et al., 2008; Steinke et al., 2010; Vázquez Riveiros et al., 2016). These works consider that the input of terrigenous material rich in

Fe–Mn-oxyhydroxides relative to biogenic carbonates affects the Fe/Ca and Mn/Ca ratios. This possibility might be the case in the western South Atlantic, which receives a contribution of highly weathered soils enriched in Fe–Mn-oxyhydroxides from adjacent South America (Govin et al., 2012). Furthermore, the cleaning protocol of Barker et al. (2003) is considered to be less efficient for removing Fe–Mn-oxyhydroxides compared to those with an additional reductive step (e.g., Martin and Lea, 2002). Steinke et al. (2010) tested both protocols in samples with much higher Fe/Ca and Mn/Ca values than ours (up to 0.96 and 1.65 mmol/mol of Fe/Ca and Mn/Ca, respectively) and found no apparent difference in Mg/Ca values. We hence conclude that our *G. inflata* Mg/Ca values and ocean temperatures derived from them are robust and not biased by extraneous phases.

Several calibrations could be applied to convert *G. inflata* Mg/Ca ratios into temperature (Elderfield and Ganssen, 2000; Anand et al., 2003; McKenna and Prell, 2004; Cléroux et al., 2008, 2013; Groeneveld and Chiessi, 2011; Regenberg et al., 2009). None of these calibrations take into account in their formulation the seawater salinity and carbonate chemistry effects. Due to this, we employed the calibration proposed by Gray and Evans (2019) that iteratively correct for these nonthermal influences. Considering that we are interested in the relative (anomaly) thermocline temperature variability caused by millennial-scale events and not in temperature absolute values, we used the multi-species ("generic") equation, which is indeed recommended for that (Gray and Evans, 2019). As there is no regional boron isotope reconstruction near to our site, we followed the correction method that uses atmospheric pCO2 to estimated seawater pH (Gray and Evans, 2019). Assuming calibration uncertainties, total uncertainty in the temperature reconstruction is around ± 1.5 °C (Gray and Evans, 2019). There is no large offset between this equation and those cited above, with the Gray and Evans (2019) calibration resulting in temperatures slightly

colder than Cléroux et al. (2008) calibration (used in Ballalai et al., 2019). We applied the temperature-$\delta^{18}O$ relationship given by the equation of Shackleton (1974) to estimate the seawater $\delta^{18}O$ composition ($\delta^{18}O_{SW}$) of the thermocline. A conversion factor of 0.27‰ was applied to convert values from the VPDB standard to VSMOW. The effect of changes in global sea level was subtracted from the $\delta^{18}O_{SW}$ values by applying the sea level correction of Grant et al. (2012). This operation yielded an ice-volume-corrected seawater oxygen isotopic composition ($\delta^{18}O_{IVC\text{-}SW}$) that we used as a proxy for relative changes in thermocline salinity. The $\delta^{18}O_{IVC\text{-}SW}$ uncertainty combines an uncertainty of 1.5 °C for the Mg/Ca (Gray and Evans, 2019) (which is equivalent to a 0.32‰ $\delta^{18}O$ change) plus an analytical error for *G. inflata* $\delta^{18}O$ calcite of 0.06‰. Thus, the propagated cumulative root-mean-square error estimated for the $\delta^{18}O_{IVC\text{-}SW}$ is around 0.32‰, consistent with other studies (e.g., Chiessi et al., 2015; Gebregiorgis et al., 2016).

2.4. Correlation between unevenly spaced climate time-series

The statistical significance of the comparison between *G. inflata* $\delta^{18}O$ of core GL-1090 and the ice-cores $\delta^{18}O$ from the North Greenland Ice Core Project (NGRIP Community Members, 2004) and the Antarctica Dronning Maud Land (EPICA/EDML Community Member, 2004) was tested applying the R package BINCOR (Polanco-martínez et al., 2019). BINCOR (BINned CORrelation) is based on a novel estimation approach proposed by Mudelsee (2014) to estimate the correlation between two unevenly spaced climate time series without the need for interpolation. BINCOR resamples the time series into time bins on a regular grid and then assigns the mean values of the variable under scrutiny within these bins. The estimated binned time series assumes the memory or persistence of the climate signal, and to do this, an autoregressive (AR1) model is fitted to each unevenly spaced time series to be analyzed (Polanco-Martínez et al., 2019). We kept most of the default BINCOR parameters, which are those in which the authors found superiority in terms of root mean square deviation on a series of Monte Carlo simulations (e.g., FLAGTAU = 3 was the rule to determine the bin-width). As BINCOR does not require interpolation, we used the original $\delta^{18}O$ of the NGRIP (6.69–119.95 ka BP) and EDML (6.69–119.04 ka BP) ice cores on the AICC2012 timescale (Bazin et al., 2013; Veres et al., 2013). The only modification was the removal of the first six thousand years of both ice cores data since the youngest *G. inflata* $\delta^{18}O$ sample in core GL-1090 is 6.69 ka BP. After the determination of the binned time-series, the Pearson correlation coefficient was estimated between GL-1090 versus NGRIP (and EDML), and the cross-correlation analysis was performed to explore the lead-lag nature of the series. Both functions are available on the BINCOR package (Polanco-Martínez et al., 2019).

3. Results

3.1. Mg/Ca-derived temperature and $\delta^{18}O_{IVF\text{-}SW}$

G. inflata $\delta^{18}O$ ranged between 0.60 and 2.33‰ for the last interglacial-glacial cycle (Fig. 3A). Two patterns of variability can be seen throughout this period. During MIS 5 (ca. 115–70 ka BP), a series of rapid millennial-scale variations occur. For example, at ca. 84 ka BP $\delta^{18}O$ decreased ca. 0.65‰ within ca. 0.4 ka. Other intervals of rapid $\delta^{18}O$ excursions can also be recognized during the early last glacial (Fig. 3A). The transition to MIS 4 (70–59 ka BP) was accompanied by dampening of such millennial-scale oscillation, and *G. inflata* $\delta^{18}O$ remained relatively constant or was affected by only minor oscillations of ca. 0.2‰ until the end of MIS 3 (29 ka BP) (Fig. 3A). MIS 4 was characterized by a significant increase in $\delta^{18}O$,

where values as high as 2.0‰ occurred. These values appeared again at the end of the Last Glacial Maximum and during the last deglaciation (19–11.7 ka BP) (Fig. 3A).

The absolute Mg/Ca-derived temperatures for MIS 5 ranged between 3.3 and 15.2 °C (Fig. 3B), with an average temperature of 10.0 °C. The onset of the last glacial during early MIS 5 (ca. 115–110 ka BP) was marked by a thermocline temperature rise of approximately 3 °C. During mid-MIS 5 (100–90 ka BP), the thermocline remained relatively cold, with a temperature around 8 °C. At late-MIS 5, thermocline temperatures were relatively warm but punctuated by rapid cold intervals, where the coldest value of 3.3 °C for MIS 5 occurred at 74.5 ka BP (Fig. 3B). Two core sections of MIS 5 (between 109.6 and 105.4 ka BP and 88.8–84.7 ka BP) did not provide enough *G. inflata* shells to perform Mg/Ca analyses (Fig. 3B). The thermocline $\delta^{18}O_{IVF\text{-}SW}$ ranged between −3.0 and 0.79‰ and is roughly parallel to thermocline temperatures with fresher (saltier) periods agreeing with intervals of colder (warmer) temperatures (Fig. 3C). The average $\delta^{18}O_{IVF\text{-}SW}$ value for MIS 5 was of −0.63‰.

3.2. Binned time series

The binned time-series for GL-1090, NGRIP, and EDML $\delta^{18}O$ are shown in Fig. 4. For the pair GL-1090 versus NGRIP, BINCOR generated binned time-series with 63 bins (Nb = 63) (Fig. 4A and B). The 63 data of the resampled time-series are spaced on a regular grid of 1.78 ka (bin-width). For the pair GL-1090 versus EDML, BINCOR generated binned time-series with 43 bins (Nb = 43) (Fig. 4C and D). The 43 data of the resampled time-series are spaced on a regular grid of 2.63 ka. The highest Pearson correlation coefficient (R) between GL-1090 and NGRIP was achieved at lag = 0 (R = −0.63; p-value ≪0.001), and the correlation progressively decrease with increasing lag. For the case of GL-1090 and EDML, the highest Pearson correlation coefficient was achieved at lag = 1 (R = −0.56; p-value = 0.003).

4. Discussion

4.1. Southern vs. northern high-latitude signal propagation to the Santos Basin

Records of the last glacial period may document abrupt millennial-scale transitions that are connected with the climate instability reported for this period (e.g., Alley et al., 2003). The way these events are organized gives a notion of coupling between different compartments of the climate system. Records related to Antarctica Isotope Maxima tend to develop a more gradual "triangular" shape in their signal, whereas those related to Greenland DO events present a more abrupt "rectangular" shape (Hinnov et al., 2002). The shape of the millennial-scale signal is a first-order indicative of uncovering southern vs. northern influence in a particular area. The *Globigerina bulloides* $\delta^{18}O$ record from the Iberian margin core MD95-2042 (37 °N) (Shackleton et al., 2000) is an excellent example of abrupt millennial-scale changes in the oceans that are coeval with DO events (Fig. 5A and B). The pervasive character of millennial-scale variability in the $\delta^{18}O$ record of this surface planktic foraminifera denotes a tight, atmospheric coupling between the mid- and high-latitudes of North Atlantic (Shackleton et al., 2000). Although shorter than MD95-2042, the *G. inflata* $\delta^{18}O$ record from the Bermuda Rise ODP Site 1063 (33 °N) also exhibits an excellent correspondence to the NGRIP $\delta^{18}O$ (Fig. 5A and C) (Thornalley et al., 2013). Unlike *G. bulloides*, *G. inflata* is a thermocline-dweller foraminifera (Cléroux et al., 2007) and the recognition of Greenland DO-like $\delta^{18}O$ variability in the subtropical Bermuda Rise likely occurred in response to freshwater-driven changes in the AMOC that were suggested to alter northward
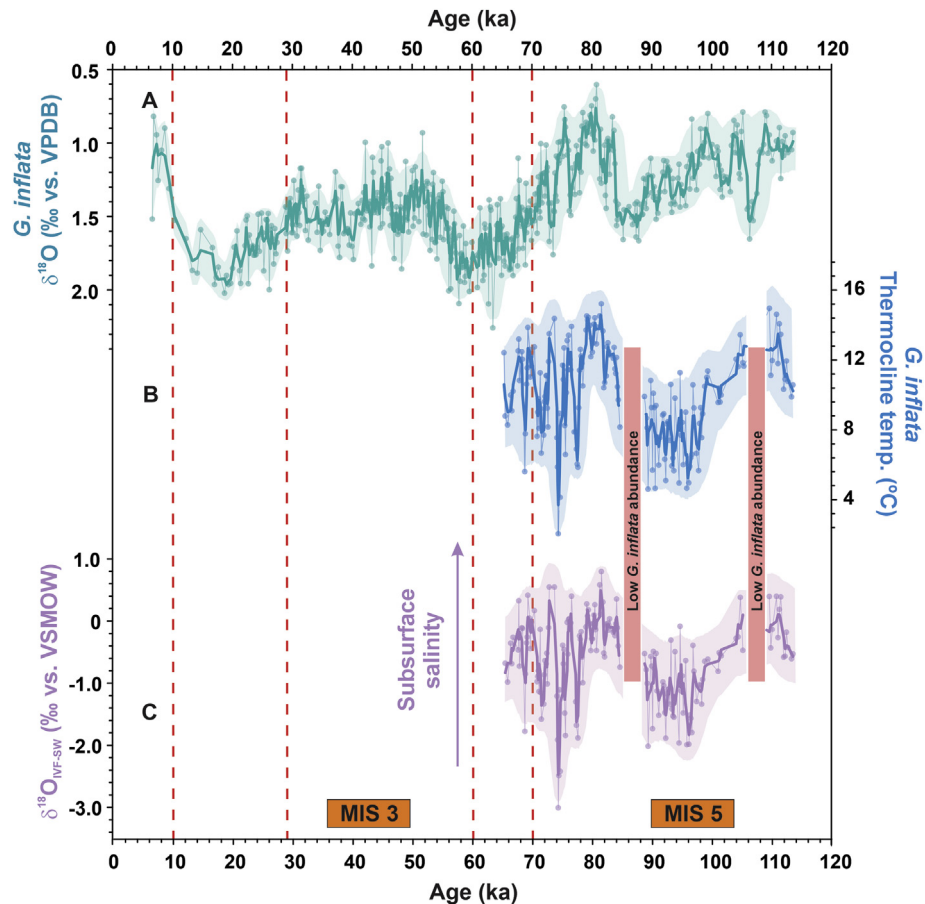
Fig. 3. Santos Basin thermocline properties based on geochemical analyses of Globorotalia inflata in core GL-1090. A: G. inflata $\delta^{18}O$. B: Thermocline temperature based on G. inflata Mg/Ca. C: Ice volume free thermocline seawater $\delta^{18}O$ ($\delta^{18}O_{IVF-SW}$) derived from the G. inflata $\delta^{18}O$ and Mg/Ca-temperature. Shading indicates the 95% confidence envelope, including age and analytical uncertainty. Red bars highlight the intervals where G. inflata was not present in enough abundance to perform Mg/Ca, and $\delta^{18}O_{IVF-SW}$ analyzes. Dashed red lines indicate the limits of Marine Isotope Stages (MIS). In this study, we emphasized MIS 5 and 3. All records are presented with a three-point running average (thick lines). (For interpretation of the references to colour in this figure legend, the reader is referred to the Web version of this article.)

heat transport in the Atlantic (Ganopolski and Rahmstorf, 2001; Schmidt et al., 2012). Similar reasoning might be applied to the *Neogloboquadrina dutertrei* $\delta^{18}O$ of the western equatorial South Atlantic core GL-1248 (0.5 °S) (Fig. 5A and D) (Venancio et al., 2018). Rapid excursions in this record have been interpreted as changes in the equatorial stratification that was simultaneous to modifications in the AMOC strength and equatorial trade winds (Venancio et al., 2018). These three cores exhibit the presence of abrupt large-amplitude $\delta^{18}O$ variability (>0.5‰) in both MIS 5 and 3, with a structure that resembles the one shown by the NGRIP ice-core (Fig. 5A−D).

Analogous to the aforementioned marine records (MD95-2042, ODP Site 1063, and GL-1248), when we compare the *G. inflata* $\delta^{18}O$ from the Santos Basin GL-1090 (24 °S − this study) with NGRIP $\delta^{18}O$ emerges a millennial-scale structure very similar to the sequence of DO cycles (Fig. 5A and E). However, our large-amplitude $\delta^{18}O$ variability is mostly constrained during MIS 5, and after the transition to full glacial conditions (MIS 4), the amplitude of the GL-1090 $\delta^{18}O$ was strongly dampened. One example of this is GI 21 (late-MIS 5), which is characterized by a rapid $\delta^{18}O$ decrease by ca. 1.0‰ in the above four marine records (Fig. 5A − E). GI 16/17 (early-MIS 3), on the other hand, only show the same type of rapid $\delta^{18}O$ decrease in the northernmost MD95-2042, ODP Site 1063, and GL-1248 (Fig. 5A − D), and is muted in GL-1090, as well as GI 14 (Fig. 5E). The DO-like pattern seems to resurge for GI 12 and 8 in GL-

1090 (mid − to late-MIS 3), however, unlike the earliest MIS 5 DO, these more recent events seem to result in a narrower $\delta^{18}O$ variability (ca. 0.2‰) compared to the ones exhibited by MD95-2042 and GL-1248 (Fig. 5B, D, and E).

The similarity in the pattern of all marine $\delta^{18}O$ records presented in Fig. 5 with NGRIP $\delta^{18}O$ suggests that feedback may have operated between the core sites and the high-latitude North Atlantic vicinities. For the GL-1090 region, such feedback was seemingly more robust during the early phase of the last glacial cycle (MIS 5), and after the transition to full glacial conditions (MIS 4), it became eventually absent (early-MIS 3) or weak (mid-to late-MIS 3). The fact that the Antarctic EDML $\delta^{18}O$ record (which shows more gradual changes and a "triangular" shape) poorly resembles the *G. inflata* $\delta^{18}O$ of GL-1090 (Fig. 5E and G) is additional support for a northern influence. The lack of an Antarctic signal in our thermocline $\delta^{18}O$ could suggest that the Southern Ocean climate did not significantly influence SACW (the water mass where *G. inflata* dwells) during abrupt millennial-scale changes in the North Atlantic or that the Southern Ocean influence is removed from the central water as it moves northward.

The reason behind abrupt transitions in *G. inflata* $\delta^{18}O$ likely resides in changes in the AMOC transport and heat content through the last glacial millennial-scale events, which affected the subtropical western South Atlantic (the mechanism for this will be discussed in the next topic). Vettoretti and Peltier (2015) and Pedro
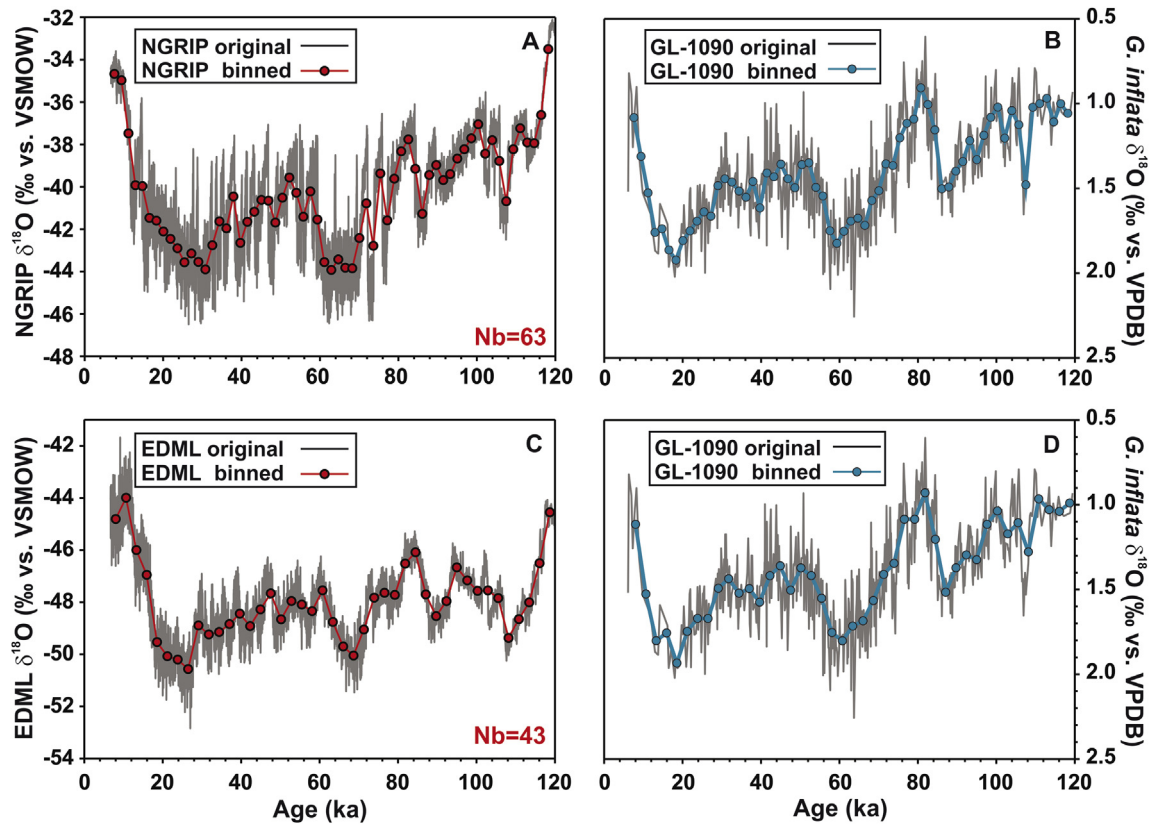
Fig. 4. Comparison between original (grey) and binned time-series (red and green) of Globorotalia inflata δ^{18}O of core GL-1090 (this study), North Greenland Ice Core Project (NGRIP Community Members, 2004) and Antarctica Dronning Maud Land (EPICA/EDML Community Members, 2004) both plotted on Antarctica Ice Core Chronology 2012 (AICC2012 - Bazin et al., 2013; Veres et al., 2013). For the first pair (panels A and B − NGRIP and GL-1090, respectively), BINCOR created binned time-series with 63 bins (Nb = 63). For the second pair (panels C and D − EDML and GL-1090, respectively), BINCOR created binned time-series with 43 bins (Nb = 43). For the first (A and B) and second (C and D) experiments, the bin-width (i.e., the spacing between data points) was 1.78 and 2.63 ka, respectively. The binning process leads to some information loss because it assumes a mean value that represents the entire variability of each individual bin (Polanco-Martínez et al., 2019). However, it is important to note that the basic structure of all δ^{18}O records was kept in the binned data. (For interpretation of the references to colour in this figure legend, the reader is referred to the Web version of this article.)

et al. (2018) through an internal oscillator applied in the North Atlantic and hosing experiments in regions of deep-water convection, respectively, simulated conditions for AMOC collapse and resumption. Although the differences in initial model configuration, both studies found a subsurface to intermediate warming of the Atlantic in moments of AMOC collapse (or the opposite during AMOC resumption) extending southward. A particular feature of these simulations is that they produce a more attenuated response for surface waters in the region of our core (zero to ca. 2 °C of temperature anomaly in the AMOC collapsed mode; Vettoretti and Peltier (2015) and Pedro et al. (2018)). A similar inference could be taken from the comparison of the *G. inflata* δ^{18}O with the same proxy measured in shells of the surface-dweller *Globigerinoides ruber* (also in GL-1090 core; Santos et al., 2017a) (Fig. 5F). The surface planktic foraminifera δ^{18}O does not show the prominent DO-like structure as the thermocline *G. inflata* does (Fig. 5E and F). Sea surface temperature derived from *G. ruber* Mg/Ca ratio in this core (Santos et al., 2017a) neither is strongly marked by millennial-scale events coeval to AMOC collapses (no positive temperature anomaly during Heinrich stadials; Santos et al. (2017a)). That is, for a forcing applied over the high-latitude North Atlantic that weakens the AMOC (Vettoretti and Peltier, 2015; Pedro et al., 2018), one would expect a more vigorous response located in the thermocline than on surface in the subtropical western South Atlantic. This is in line with what proxy data indicate (Fig. 5E and F). Such good agreement between models that simulate perturbations in the northern cell of the AMOC and our reconstruction is a piece of

additional evidence to consider that the *G. inflata* δ^{18}O is likely being modulated by patterns connected with the North Atlantic circulation (at the expense of coupling with the Southern Ocean).

To further investigate the correlation between the Santos Basin thermocline and Greenland and Antarctica climate, we applied the correlation tools of BINCOR over the binned time-series. Fig. 6A shows that the binned time-series of GL-1090 and NGRIP inversely covary, especially during MIS 5. The main exception is the time interval between 40 and 20 ka BP (Fig. 6A). Nevertheless, the relationship between GL-1090 and NGRIP gives a strong negative correlation (R = −0.63) that reaches its maximum at lag = 0 (Fig. 6B and C). The bin-width for the pair GL-1090-NGRIP (1.78 ka) falls well within the age uncertainties for both MIS 5 and 3 (section 2.2 and Fig. 2B) of 1.87 and 1.71 ka, respectively. This denotes a close link of NGRIP DO variability and the *G. inflata* δ^{18}O of the thermocline western South Atlantic. For the binned time-series of GL-1090 and EDML, a lower correspondence is seen (Fig. 6D). Additionally, we find a significant yet lower negative correlation (R = −0.56) at lag = 1, which suggests a lead of 2.6 kyr of Antarctica (Fig. 6E and F). This apparent "southern lead" was discussed in detail by Schmittner et al. (2003) for modeling experiments with ice-cores δ^{18}O. In this study, the authors discarded the "southern lead" mechanism and suggested that the coupling of the hemispheres at the millennial time-scale would be more readily explained by a trigger in the North Atlantic. The higher correlation attained at lag = 0 (r = −0.63) between the *G. inflata* δ^{18}O and NGRIP allows us to follow a similar conclusion.
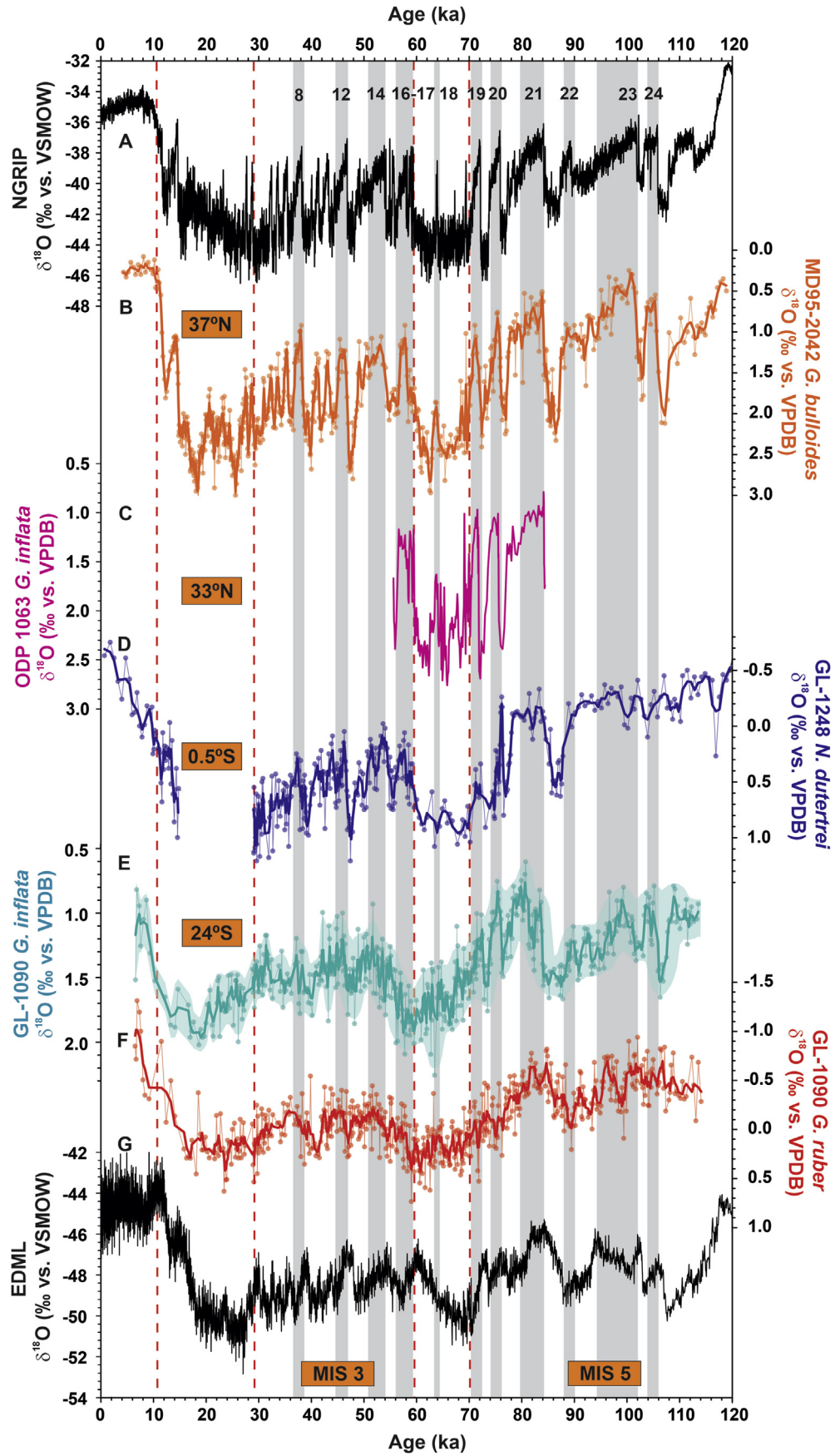
Schmittner et al. (2003) found a time lag of 300−400 years in Antarctica relative to Greenland. The recently drilled West Antarctica Divide ice-core indicates the strongest anti-correlation between Greenland warming and Antarctica cooling at a Northern Hemisphere lead of only 218 years (Wais Divide Project, 2013). Both studies rely on a north-to-south directionality of the abrupt millennial time-scale events to the Southern Ocean by oceanic processes. However, as highlighted by Schmittner et al. (2003), most of the lag in the signal transmission to Antarctica occurs between 40 and 60 °S due to the effective barrier imposed by the Antarctic Circumpolar Current. Upstream between 20 and 40 °S, the abrupt warming during GI would result in thermocline South Atlantic cooling almost simultaneously (Schmittner et al., 2003). The simulations of the DO oscillations developed by Vettoretti and Peltier (2015) also provide support for rapid north-to-south transmission of abrupt millennial-scale variability through the Atlantic thermocline, with temperatures at 250 m depth in the South Atlantic presenting only a short lag relative to Greenland. This could explain the highest correlation between GL-1090 and NGRIP be attained at lag = 0 (Fig. 6C). Based on the main findings of these studies, plus the similar DO shape imprinted in *G. inflata* δ^{18}O and the higher correlation found at lag = 0 (r = −0.63), we assume that the millennial-scale pattern apparent in our data is the result of southward propagation of the North Atlantic DO variability that influenced the thermocline SACW in the subtropical western South Atlantic but with an asymmetrical intensity through the last glacial cycle.

4.2. Differences between MIS 5 and 3 associated with changes in the meridional extension of the thermocline heat reservoir

The connection between the northern high-latitude climate and South Atlantic could be proportioned by the vertical displacement of the isopycnals associated with Kelvin wave propagation traveling along the western boundary of the Atlantic (Stocker and Johnsen, 2003). Such isopycnal displacement could be generated in response to a thermocline warm pool anomaly during GS (or the opposite during GI) that can span Atlantic subtropical latitudes (Vettoretti and Peltier, 2015). Different from the findings from modeling studies, our data indicate that the response of the thermocline subtropical western South Atlantic was not monotonous for all millennial-scale events since MIS 5 DO were accompanied by *G. inflata* δ^{18}O amplitudes much broader than those of MIS 3.

In the experiments of Vettoretti and Peltier (2015) and Pedro et al. (2018), a thermal reservoir through Atlantic thermocline is well developed until ca. 40 °S during intervals of AMOC reduction. A meridional extension like that could easily incorporate the GL-1090 site. However, as shown by Buizert and Schmittner (2015), DO events are not uniformly distributed, and those occurring in MIS 5 tend to be longer than those of MIS 3. If the heat reservoir were produced at the tail of a GS, it would be expected that it would maintain some proportionality with the intensity/duration of a particular stadial. This could mean that not all GS would result in a heat reservoir extending until ca. 40 °S. Variations in the southern extension of the Atlantic thermocline heat reservoir could explain

why *G. inflata* δ^{18}O from GL-1090 has asymmetric responses throughout the last glacial period. During MIS 5, the site of GL-1090 would be fully embedded by such a reservoir (or even close to its core), while during MIS 3, the region would not be influenced (early-MIS 3) or would be located barely near to its southern boundary (mid-to late-MIS 3).

This scenario fits the circulation schemes proposed by Bereiter et al. (2012) to explain discrepancies between millennial-scale events of CO_2 release from the ocean to the atmosphere between MIS 5 and 3. According to these authors, MIS 5 GI was superimposed on a modern-like circulation state so that the production of deep NADW remained nearly steady (or even intensified during a warm event). On the other hand, MIS 3 DO events took place on a colder glacial background, where northern high-latitude convection produced a shallower Glacial North Atlantic Intermediate Water (Bereiter et al., 2012). A forcing applied to the ocean to disturb the AMOC in the MIS 5 condition of Bereiter et al. (2012) should be necessarily higher compared to the MIS 3 condition, where the background already produces a sluggish circulation. Consequently, it is reasonable to expect heat reservoirs better established in the Atlantic during stadials of MIS 5. Besides, a northward shift of the Antarctic Circumpolar Current and associated fronts with the advance of the glacial climate from MIS 5 to 3 could limit the southward extension of the heat reservoir.

The MIS 5 GS in NGRIP δ^{18}O is characterized by excursions to values below − 40‰ (Fig. 7A). These cold intervals in Greenland were followed by weaker ventilation, and the presence of more radiogenic southern sourced waters in the deep North Atlantic revealed by benthic δ^{13}C and neodymium isotopes of MD95-2042 and ODP Site 1063, respectively (Shackleton et al., 2000; Govin et al., 2014; Böhm et al., 2015) (Fig. 7B). The pattern of *G. bulloides* δ^{18}O increase during MIS 5 GS can be interpreted to reflect mostly surface temperature variations at the location of MD95-2042 (Shackleton et al., 2000, Fig. 7C). These data reflect recurrent events of AMOC slowdown that tend to increase North Atlantic subsurface to intermediate temperatures (Jonkers et al., 2010; Marcott et al., 2011; Alvarez-Solas et al., 2013; Ezat et al., 2014; Rasmussen et al., 2016).

In general, our thermocline Mg/Ca results from the Santos Basin are consistent with this line of interpretation, which is seen during GS 21 and 20 (Fig. 7E). During these Greenland cold events, western South Atlantic thermocline temperatures reconstructed in GL-1090 were approximately 3 °C warmer than the average. A simultaneous rise in thermocline salinity is also indicated by the δ^{18}O$_{IVF-SW}$ that became 0.6‰ higher during these GS (Fig. 7E and F). This magnitude of warming is similar to the one reproduced by transient simulations with the Community Climate System Model, where South Atlantic temperatures at the apparent calcification depth of *G. inflata* (ca. 400 m water depth; Chiessi et al., 2007) warmed by 2−4 °C in response to an AMOC collapse (Pedro et al., 2018). According to Pedro et al. (2018), the heat content of the South Atlantic increases due to a (i) 50−100 m thermocline deepening within a century of AMOC collapse, and (ii) reduced northward advection of heat in the AMOC upper limb. During GS 25 and 22, this thermocline deepening may have been pronounced enough to disturb

Fig. 5. Comparison between Greenland and Antarctica ice-core δ^{18}O with North and South Atlantic marine sediment core δ^{18}O. A: North Greenland Ice Core Project δ^{18}O (NGRIP Community Members, 2004) plotted on Antarctica Ice Core Chronology 2012 (AICC2012 - Bazin et al., 2013; Veres et al., 2013). B: *Globigerina bulloides* δ^{18}O of core MD95-2042 (Shackleton et al., 2000) plotted on the AICC2012 time-scale after Govin et al. (2014). C: *Globorotalia inflata* δ^{18}O of ODP Site 1063 (Thornalley et al., 2013). D: *Neogloboquadrina dutertrei* δ^{18}O of core GL-1248 (Venancio et al., 2018). E: *Globorotalia inflata* δ^{18}O of core GL-1090 (this study). F: *Globigerinoides ruber* δ^{18}O of core GL-1090 (Santos et al., 2017a). G: Antarctica Dronning Maud Land δ^{18}O (EPICA/EDML Community Member, 2004) plotted on AICC2012. Shading indicates the 95% confidence envelope, including age and analytical uncertainty. Grey bars highlight millennial-scale variability associated with Greenland interstadials. Dashed red lines indicate the limits of Marine Isotope Stages (MIS). In this study, we concentrate on MIS 3 and 5. Records of panels B, D, E, and F are presented with three-point running averages (thick lines). Note that the highlighted DO cycles of MIS 3 did not produce a clear signal of millennial-scale variability in the *G. inflata* δ^{18}O of core GL-1090, unlike the DO cycles of MIS 5. (For interpretation of the references to colour in this figure legend, the reader is referred to the Web version of this article.)
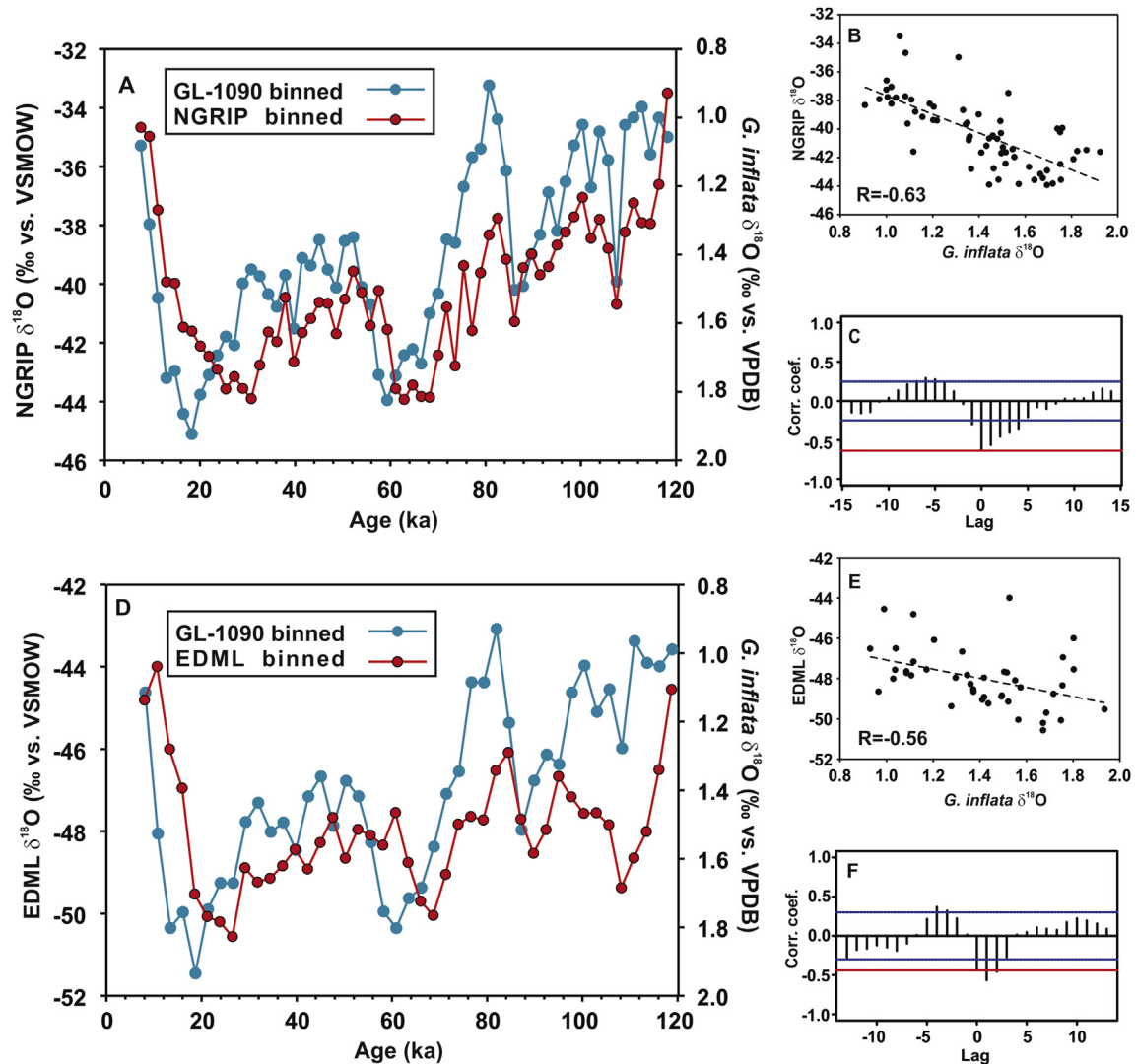
Fig. 6. Correlation analyses between the binned time-series generated for *Globorotalia inflata* δ18O of GL-1090 (this study), North Greenland Ice Core Project δ18O (NGRIP Community Members, 2004) and Antarctica Dronning Maud Land δ18O (EPICA/EDML Community Member, 2004) plotted on Antarctica Ice Core Chronology 2012 (AICC2012 - Bazin et al., 2013; Veres et al., 2013). A and D: binned δ18O of GL-1090 (green) and NGRIP (red) (A) and EDML (red) (D). B and E: Pearson linear correlation (dashed black line) for GL-1090 versus NGRIP (B) and GL-1090 versus EDML (E). C and F: cross-correlation for GL-1090 versus NGRIP (C) and GL-1090 versus EDML (F). Blue and red lines on panels C and F denote the 95% confidence intervals and the correlation value at lag = 0, respectively. Note that for the cross-correlation between GL-1090 and NGRIP (C), the highest correlation coefficient coincides with lag = 0. (For interpretation of the references to colour in this figure legend, the reader is referred to the Web version of this article.)

G. inflata populations in SACW, explaining its low abundance in the Santos Basin sediments. GS 25 and 22 hold some of the most extensive excursions in the *G. inflata* and *G. bulloides* δ18O of GL-1090 and MD95-2042 (Fig. 7C and D), as well as in the benthic δ13C of MD95-2042 and neodymium isotopes of ODP1063 (Fig. 7B). This suggests that they were associated with more considerable changes in the northward heat transport compared to other MIS 5 GS.

On the other hand, the rapid reinvigoration of the overturning during GI swings the thermocline western South Atlantic temperature and salinity in the opposite direction (Fig. 7E and F). This recovery is generally connected to the disruption of the sharp density gradient created due to the presence of warm waters below a thin cold tongue at the surface North Atlantic during stadials. The collapse of this density inversion induced a fast release of the stored heat to the atmosphere cooling the thermocline layer (Mignot et al., 2007). Our temperature reconstruction shows that some MIS 5 GI was associated with a ca. 4 °C cooling (or higher in the case of GI 20)

in the thermocline western South Atlantic. Coherently, the longest MIS 5 interstadial, GI 23, was followed by a prolonged cooling in the study region. The apparent exception to this pattern was GI 24 and 21 when the temperature remained above its average. However, both intervals follow a gap in the *G. inflata* Mg/Ca record, and the temperature for GS 25 and 22 is unknown (Fig. 7E and F). It is theoretically possible that GS 25 and 22 were so warm that even the subsequent cooling did not result in temperatures below the average during GI 24 and 21, respectively.

Adjustments in the AMOC strength propagated a north-to-south DO signal through the western Atlantic that was imprinted in the shells of the thermocline dwelling *G. inflata* more clearly during the early part of the last glacial cycle. Although we cannot completely rule out the occurrence of DO-related temperature and salinity fluctuations during MIS 3 in this region, if they occurred, they were likely of smaller magnitude since the abrupt millennial-scale signal was mostly dampened from the *G. inflata* δ18O. We argue that the GI of MIS 5 was fueled by heat accumulated from latitudes as far south

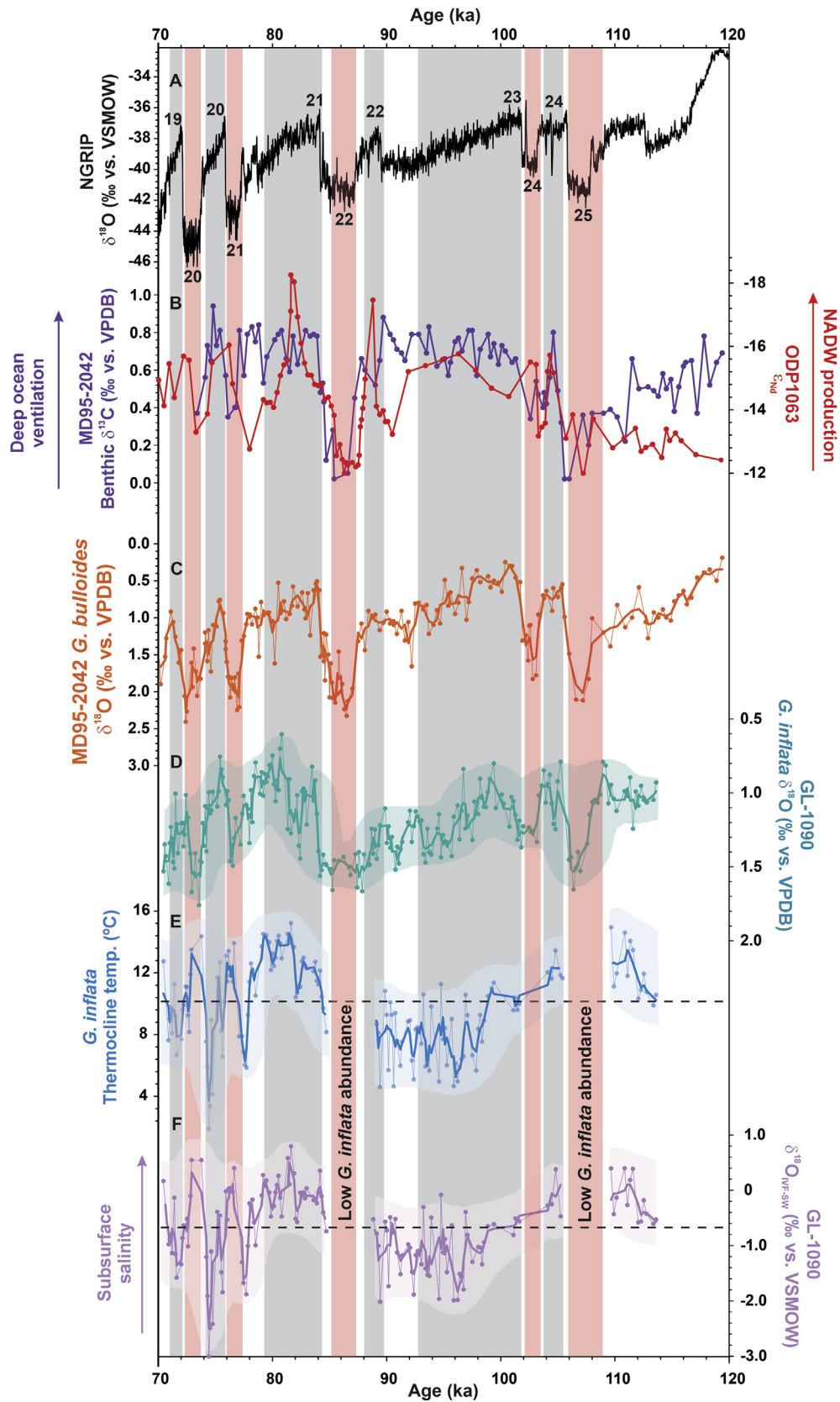**Fig. 7.** Climatic evolution of Marine Isotope Stage (MIS) 5 based on NGRIP ice-core and Atlantic records. A: North Greenland Ice Core Project δ¹⁸O (NGRIP Community Members, 2004) plotted on Antarctica Ice Core Chronology 2012 (AICC2012 - Bazin et al., 2013; Veres et al., 2013). B: *Cibicides* spp. δ¹³C of core MD95-2042 (Shackleton et al., 2000) plotted on AICC2012 time-scale after Govin et al. (2014) (purple) and neodymium isotope of ODP1063 (Böhm et al., 2015) (red). C: *Globigerina bulloides* δ¹⁸O of core MD95-2042 (Shackleton et al., 2000) plotted on the AICC2012 time-scale after Govin et al. (2014). D: *Globorotalia inflata* δ¹⁸O of core GL-1090 (this study). E: Thermocline temperature based on *G. inflata* Mg/Ca (this study). F: Subsurface δ¹⁸O_IVF-SW derived from *G. inflata* δ¹⁸O and Mg/Ca-temperature. Dashed lines on panels E and F indicate the average values for thermocline temperature and δ¹⁸O_IVF-SW, respectively. Shading indicates the 95% confidence envelope, including age and analytical uncertainty. Grey and red bars highlight millennial-scale variability associated with Greenland interstadials and stadials, respectively. (For interpretation of the references to colour in this figure legend, the reader is referred to the Web version of this article.)

as 24 °S while the GI of MIS 3 relied on a narrower meridional heat reservoir in the Atlantic that marginally affected the Santos Basin thermocline $\delta^{18}O$. This could be one of the reasons behind the shorter interstadial durations during MIS 3 compared to MIS 5.

5. Conclusions

We reconstructed the thermocline conditions of the subtropical western South Atlantic based on the $\delta^{18}O$ and Mg/Ca ratio of deep-dwelling planktic foraminifera *G. inflata* in order to reveal the impacts of last glacial millennial-scale events in this region, as previously demonstrated by model simulations. Taking into account age model uncertainties, our high-resolution *G. inflata* $\delta^{18}O$ record shows distinct abrupt millennial-scale changes that strongly resemble the sequence of GI/GS events, which impacted the region more significantly during MIS 5 than during MIS 3. Cross-correlation analyses between the Santos Basin thermocline $\delta^{18}O$ and ice-cores (NGRIP and EDML) suggest that the Santos Basin thermocline was affected by the AMOC disruptions following DO cycles at almost no lag. Thermocline temperature and $\delta^{18}O_{IVF-SW}$ reconstruction during MIS 5 indicate higher temperature and salinity during GS 21 and 20 (and likely during Greenland stadials 25 and 22), agreeing with model studies that consider this region as a heat reservoir at times of weakened AMOC. The opposite pattern occurs during GI 23, 20, and 19. The dampened or absent DO-like signal in the *G. inflata* $\delta^{18}O$ during MIS 3 suggests an asymmetric response of the region throughout the last glacial. We argue that the MIS 3 DO events were not accompanied by disturbances in the northward heat transport as far-reaching as those of MIS 5, leading us to conclude that these youngest DO cycles were supported by a smaller heat and salt reservoir in the Atlantic. This could be one of the reasons for the shorter interstadial durations during MIS 3 compared to MIS 5. High-resolution thermocline temperature of MIS 3 in the subtropical western South Atlantic should be tested in the future to ascertain this possibility.

Declaration of competing interest

The authors declare that they have no known competing financial interests or personal relationships that could have appeared to influence the work reported in this paper.

CRediT authorship contribution statement

Thiago P. Santos: Writing - original draft. **João M. Ballalai:** Formal analysis. **Daniel R. Franco:** Investigation, Software. **Rômulo R. Oliveira:** Investigation, Software. **Douglas O. Lessa:** Conceptualization, Writing - review & editing. **Igor M. Venancio:** Conceptualization, Writing - review & editing. **Cristiano M. Chiessi:** Conceptualization, Writing - review & editing. **Henning Kuhnert:** Resources, Writing - review & editing. **Heather Johnstone:** Resources, Writing - review & editing. **Ana Luiza S. Albuquerque:** Supervision, Project administration, Funding acquisition.

Acknowledgments

Appendix A. Supplementary data

Supplementary data to this article can be found online at https://doi.org/10.1016/j.quascirev.2020.106307.

References

Alley, R.B., Anandakrishnan, S., Jung, P., 2001. Stochastic resonance in the north atlantic. Paleoceanography 16, 190–198. https://doi.org/10.1029/2000PA000518.

Alley, R.B., Marotzke, J., Nordhaus, W.D., Overpeck, J.T., Peteet, D.M., Pielke, R.A., Pierrehumbert, R.T., Rhines, P.B., Stocker, T.F., Talley, L.D., Wallace, J.M., 2003. Abrupt climate change. Science 299. https://doi.org/10.1126/science.1081056, 2005–10.

Alvarez-Solas, J., Charbit, S., Ritz, C., Paillard, D., Ramstein, G., Dumas, C., 2010. Links between ocean temperature and iceberg discharge during Heinrich events. Nat. Geosci. 3, 122–126. https://doi.org/10.1038/ngeo752.

Alvarez-Solas, J., Robinson, A., Montoya, M., Ritz, C., 2013. Iceberg discharges of the last glacial period driven by oceanic circulation changes. Proc. Natl. Acad. Sci. U.S.A. 110, 16350–16354. https://doi.org/10.1073/pnas.1306622110.

Anand, P., Elderfield, H., Conte, M.H., 2003. Calibration of Mg/Ca thermometry in planktonic foraminifera from a sediment trap time series. Paleoceanography 18. https://doi.org/10.1029/2002PA000846 n/a-n/a.

Angulo, R.J., Reimer, P.J., de Souza, M.C., Sheel-Ybert, R., Tenorio, M.C., Disaro, S.T., Gaspar, M.D., 2007. A tentative determination of upwelling influence on the paleo-surficial marine water reservoir effect in southeastern Brazil AN. Radiocarbon 49, 1255–1259.

Ballalai, J.M., Santos, T.P., Lessa, D.O., Venancio, I.M., Chiessi, C.M., Johnstone, H.J.H., Kuhnert, H., Claudio, M.R., Toledo, F., Costa, K.B., Albuquerque, A.L.S., 2019. Tracking spread of the Agulhas leakage into the western South atlantic and its northward transmission during the last interglacial. Paleoceanogr. Paleoclimatol. https://doi.org/10.1029/2019PA003653, 2019PA003653.

Barker, S., Greaves, M., Elderfield, H., 2003. A study of cleaning procedures used for foraminiferal Mg/Ca paleothermometry. Geochemistry, Geophys. Geosystems 4, 1–20. https://doi.org/10.1029/2003GC000559.

Bay, Ryan, Bramall, Nathan, Buford Price, P, 2004. Bipolar correlation of volcanism with millennial climate change. Proceedings of the National Academy of Sciences of the United States of America 101 (17), 6341–6345. https://doi.org/10.1073/pnas.0400323101.

Bazin, L., Landais, A., Lemieux-Dudon, B., Toyé Mahamadou Kele, H., Veres, D., Parrenin, F., Martinerie, P., Ritz, C., Capron, E., Lipenkov, V., Loutre, M.F., Raynaud, D., Vinther, B., Svensson, A., Rasmussen, S.O., Severi, M., Blunier, T., Leuenberger, M., Fischer, H., Masson-Delmotte, V., Chappellaz, J., Wolff, E., 2013. An optimized multi-proxy, multi-site Antarctic ice and gas orbital chronology (AICC2012): 120-800 ka. Clim. Past 9, 1715–1731. https://doi.org/10.5194/cp-9-1715-2013.

Bereiter, B., Luthi, D., Siegrist, M., Schupbach, S., Stocker, T.F., Fischer, H., 2012. Mode change of millennial CO_2 variability during the last glacial cycle associated with a bipolar marine carbon seesaw. Proc. Natl. Acad. Sci. Unit. States Am. 109, 9755–9760. https://doi.org/10.1073/pnas.1204069109.

Blaauw, M., Christen, J.A., Bennett, K.D., Reimer, P.J., 2018. Double the dates and go for Bayes — impacts of model choice, dating density and quality on chronologies. Quat. Sci. Rev. 188, 58–66. https://doi.org/10.1016/j.quascirev.2018.03.032.

Blaauw, M., Christeny, J.A., 2011. Flexible paleoclimate age-depth models using an autoregressive gamma process. Bayesian Anal. 6, 457–474. https://doi.org/10.1214/11-BA618.

Blunier, T., Brook, E.J., 2001. Timing of millennial-scale climate change in Antarctica and Greenland during the last glacial period. Science 291, 109–112. https://doi.org/10.1126/science.291.5501.109.

Böhm, E., Lippold, J., Gutjahr, M., Frank, M., Blaser, P., Antz, B., Fohlmeister, J., Frank, N., Andersen, M.B., Deininger, M., 2015. Strong and deep Atlantic meridional overturning circulation during the last glacial cycle. Nature 517, 73–76. https://doi.org/10.1038/nature14059.

Braun, H, Ditlevsen, P, Chialvo, D, 2008. Solar forced Dansgaard-Oeschger events and their phase relation with solar proxies. Geophysical Research Letters 35 (6), 1–5. https://doi.org/10.1029/2008GL033414.

Broecker, W.S., Andree, M., Bonani, G., Wolfli, W., Oeschger, H., Klas, M., 1988. Can the Greenland climatic jumps be identified in records from Ocean and Land? Quat. Res. 30, 1–16. https://doi.org/10.1016/0033-5894(88)90082-8.

Buizert, C., Schmittner, A., 2015. Southern Ocean control of glacial AMOC stability and Dansgaard-Oeschger interstadial duration. Paleoceanography 30, 1595–1612. https://doi.org/10.1002/2015PA002795.

Caesar, L., Rahmstorf, S., Robinson, A., Feulner, G., Saba, V., 2018. Observed fingerprint of a weakening Atlantic Ocean overturning circulation. Nature 556, 191–196. https://doi.org/10.1038/s41586-018-0006-5.

Chapman, M.R., Shackleton, N.J., 1998. Millennial-scale fluctuations in North Atlantic heat flux during the last 150,000 years. Earth Planet Sci. Lett. 159, 57–70. https://doi.org/10.1016/S0012-821X(98)00068-5.

Chiessi, C.M., Eulrich, S., Mulitza, S., Patzold, J., Wefer, L., 2007. Signature of Brazil-Malvinas Confluence Argentine Basin in the isotopic composition of planktonic foraminifera form surface sediments. Mar. Micropaleontol. 64, 52–66.

Chiessi, C.M., Mulitza, S., Mollenhauer, G., Silva, J.B., Groeneveld, J., Prange, M., 2015. Thermal evolution of the western South Atlantic and the adjacent continent during Termination 1. Clim. Past 11, 915–929. https://doi.org/10.5194/cp-11-915-2015.

Cléroux, C., Cortijo, E., Anand, P., Labeyrie, L., Bassinot, F., Caillon, N., Duplessy, J.-C., 2008. Mg/Ca and Sr/Ca ratios in planktonic foraminifera: proxies for upper water column temperature reconstruction. Paleoceanography 23. https://doi.org/10.1029/2007PA001505.

Cléroux, C., Cortijo, E., Duplessy, J.C., Zahn, R., 2007. Deep-dwelling foraminifera as thermocline temperature recorders. Geochemistry, Geophys. Geosystems 8. https://doi.org/10.1029/2006GC001474.

Cléroux, C., Demenocal, P., Arbuszewski, J., Linsley, B., 2013. Reconstructing the upper water column thermal structure in the Atlantic Ocean. Paleoceanography 28, 503–516. https://doi.org/10.1002/palo.20050.

Crowley, T.J., 1992. North Atlantic deep water cools the southern hemisphere. Paleoceanography 7, 489–497. https://doi.org/10.1029/92PA01058.

Deplazes, G., Lückge, A., Peterson, L.C., Timmermann, A., Hamann, Y., Hughen, K.A., Röhl, U., Laj, C., Cane, M.A., Sigman, D.M., Haug, G.H., 2013. Links between tropical rainfall and North Atlantic climate during the last glacial period. Nat. Geosci. 6, 1–5. https://doi.org/10.1038/ngeo1712.

Ditlevsen, P.D., Johnsen, S.J., 2010. Tipping points: early warning and wishful thinking. Geophys. Res. Lett. 37, 2–5. https://doi.org/10.1029/2010GL044486.

Dokken, T.M., Nisancioglu, K.H., Li, C., Battisti, D.S., Kissel, C., 2013. Dansgaard-Oeschger cycles: interactions between ocean and sea ice intrinsic to the Nordic seas. Paleoceanography 28, 491–502. https://doi.org/10.1002/palo.20042.

Elderfield, H., Ganssen, G., 2000. Past temperature and δ18O of surface ocean waters inferred from foraminiferal Mg/Ca ratios. Nature 405, 442–445. https://doi.org/10.1038/35013033.

Elliot, M., Labeyrie, L., Duplessy, J., 2002. Changes in North Atlantic deep-water formation associated with the Dansgaard − oeschger temperature oscillations (60 − 10 ka), 21, 1153−1165.

EPICA Community Members, 2004. Eight glacial cycles from an Antarctic ice core. Nature 429, 623–628.

Ezat, M.M., Rasmussen, T.L., Groeneveld, J., 2014. Persistent intermediate water warming during cold stadials in the southeastern Nordic seas during the past 65 k. y. Geology 42, 663–666. https://doi.org/10.1130/G35579.1.

Ganopolski, A., Rahmstorf, S., 2001. Rapid changes of glacial climate simulated in a coupled climate model. Nature 409, 153–158. https://doi.org/10.1038/35051500.

Garzoli, S.L., Matano, R., 2011. the South atlantic and the atlantic meridional overturning circulation. Deep Sea Res. Part II Top. Stud. Oceanogr. 58, 1837–1847. https://doi.org/10.1016/j.dsr2.2010.10.063.

Gebregiorgis, D., Hathorne, E.C., Sijinkumar, A.V., Nagender Nath, B., Nürnberg, D., Frank, M., 2016. South Asian summer monsoon variability during the last ~54 kyrs inferred from surface water salinity and river run off proxies. Quat. Sci. Rev. 138, 6–15. https://doi.org/10.1016/j.quascirev.2016.02.012.

Genty, D., Blamart, D., Ouahdi, R., Gilmour, M., Baker, a, Jouzel, J., Van-Exter, S., 2003. Precise dating of Dansgaard-Oeschger climate oscillations in western Europe from stalagmite data. Nature 421, 833–837. https://doi.org/10.1038/nature01391.

Gottschalk, J., Skinner, L.C., Misra, S., Waelbroeck, C., Menviel, L., Timmermann, A., 2015. Abrupt changes in the southern extent of North atlantic deep water during dansgaard−oeschger events. Nat. Geosci. 8, 950–954. https://doi.org/10.1038/ngeo2558.

Govin, A., Chiessi, C.M., Zabel, M., Sawakuchi, A.O., Heslop, D., Hörner, T., Zhang, Y., Mulitza, S., 2014. Terrigenous input off northern South America driven by changes in Amazonian climate and the North Brazil Current retroflection during the last 250 ka. Clim. Past 10, 843–862. https://doi.org/10.5194/cp-10-843-2014.

Govin, A., Holzwarth, U., Heslop, D., Ford Keeling, L., Zabel, M., Mulitza, S., Collins, J.A., Chiessi, C.M., 2012. Distribution of major elements in Atlantic surface sediments (36°N-49°S): imprint of terrigenous input and continental weathering. Geochemistry, Geophys. Geosystems 13. https://doi.org/10.1029/2011GC003785.

Grant, K.M., Rohling, E.J., Bar-Matthews, M., Ayalon, A., Medina-Elizalde, M., Ramsey, C.B., Satow, C., Roberts, A.P., 2012. Rapid coupling between ice volume and polar temperature over the past 150,000 years. Nature 491, 744–747. https://doi.org/10.1038/nature11593.

Gray, W.R., Evans, D., 2019. Nonthermal influences on Mg/Ca in planktonic foraminifera: a review of culture studies and application to the last glacial maximum. Paleoceanogr. Paleoclimatol. 34, 306–315. https://doi.org/10.1029/2018PA003517.

Greaves, M., Barker, S., Daunt, C., Elderfield, H., 2005. Accuracy, standardization, and interlaboratory calibration standards for foraminiferal Mg/Ca thermometry. Geochemistry, Geophys. Geosystems 6, 1–9. https://doi.org/10.1029/2004GC000790.

Groeneveld, J., Chiessi, C.M., 2011. Mg/Ca of Globorotalia inflata as a recorder of permanent thermocline temperatures in the South Atlantic. Paleoceanography 26, 1–12. https://doi.org/10.1029/2010PA001940.

Groeneveld, J., Nürnberg, D., Tiedemann, R., Reichart, G.-J., Steph, S., Reuning, L., Crudeli, D., Mason, P., 2008. Foraminiferal Mg/Ca increase in the caribbean during the pliocene: western atlantic warm pool formation, salinity influence, or diagenetic overprint? Geochemistry, Geophys. Geosystems 9. https://doi.org/10.1029/2006GC001564.

Hagen, S., Keigwin, L.D., 2002. Sea-surface temperature variability and deep water reorganisation in the subtropical North Atlantic during isotope stage 2-4. Mar. Geol. 189, 145–162. https://doi.org/10.1016/S0025-3227(02)00327-4.

Henry, L.G., McManus, J.F., Curry, W.B., Roberts, N.L., Piotrowski, A.M., Keigwin, L.D., 2016. North Atlantic ocean circulation and abrupt climate change during the last glaciation. Science 80 (353), 470–474. https://doi.org/10.1126/science.aaf5529.

Hinnov, L.A., Schulz, M., Yiou, P., 2002. Interhemispheric space − time attributes of the Dansgaard − oeschger oscillations between 100 and 0 ka. Quat. Sci. Rev. https://doi.org/10.1016/S0277-3791(01)00140-8.

Jonkers, L., Moros, M., Prins, M.A., Dokken, T., Dahl, C.A., Dijkstra, N., Perner, K., Brummer, G.-J.A., 2010. A reconstruction of sea surface warming in the northern North Atlantic during MIS 3 ice-rafting events. Quat. Sci. Rev. 29, 1791–1800. https://doi.org/10.1016/j.quascirev.2010.03.014.

Knorr, G., Lohmann, G., 2003. Southern Ocean origin for the resumption of Atlantic thermohaline circulation during deglaciation. Nature 424, 532–536. https://doi.org/10.1038/nature01855.

Kroopnick, P.M., 1985. The distribution of 13C of ΣCO2 in the world oceans. Deep Sea Res. Part A. Oceanogr. Res. Pap. 32, 57–84. https://doi.org/10.1016/0198-0149(85)90017-2.

Kuhnert, H., Kuhlmann, H., Mohtadi, M., Meggers, H., Baumann, K., Pätzold, J., 2014. Holocene Tropical Western Indian Ocean Sea Surface Temperatures in Covariation with Climatic Changes in the Indonesian Region 1–15. https://doi.org/10.1002/2013PA002555.Received.

Lea, D.W., Pak, D.K., Paradis, G., 2005. Influence of volcanic shards on foraminiferal Mg/Ca in a core from the Galápagos region. Geochemistry, Geophys. Geosystems 6, 1–13. https://doi.org/10.1029/2005GC000970.

Lisiecki, L.E., Raymo, M.E., 2005. A Pliocene-Pleistocene stack of 57 globally distributed benthic δ18O records. Paleoceanography 20, 1–17. https://doi.org/10.1029/2004PA001071.

Liu, W., Xie, S.-P., Liu, Z., Zhu, J., 2017. Overlooked possibility of a collapsed atlantic meridional overturning circulation in warming climate. Sci. Adv. 3, e1601666 https://doi.org/10.1126/sciadv.1601666.

Locarnini, R.A., Mishonov, A.V., Antonov, J.I., Boyer, T.P., Garcia, H.E., Baranova, O.K., Zweng, M.M., Paver, C.R., Reagan, J.R., Johnson, D.R., Hamilton, M., Seidov, D., 2013. World ocean atlas 2013, volume 1: temperature. In: Levitus, S., Mishonov Technical, A. (Eds.), NOAA Atlas NESDIS, vol. 73, p. 40.

Lohmann, J., Ditlevsen, P.D., 2018. Random and externally controlled occurrences of Dansgaard-Oeschger events. Clim. Past 14, 609–617. https://doi.org/10.5194/cp-14-609-2018.

Marcott, S.A., Clark, P.U., Padman, L., Klinkhammer, G.P., Springer, S.R., Liu, Z., Otto-Bliesner, B.L., Carlson, A.E., Ungerer, A., Padman, J., He, F., Cheng, J., Schmittner, A., 2011. Ice-shelf collapse from subsurface warming as a trigger for Heinrich events. Proc. Natl. Acad. Sci. U.S.A. 108, 13415–13419. https://doi.org/10.1073/pnas.1104772108.

Martin, P.A., Lea, D.W., 2002. A simple evaluation of cleaning procedures on fossil benthic foraminiferal Mg/Ca. Geochemistry, Geophys. Geosystems 3, 1–8. https://doi.org/10.1029/2001GC000280.

McKenna, V.S., Prell, W.L., 2004. Calibration of the Mg/Ca of Globorotalia truncatulinoides (R) for the reconstruction of marine temperature gradients. Paleoceanography 19, 1–12. https://doi.org/10.1029/2000PA000604.

Mignot, J., Ganopolski, A., Levermann, A., 2007. Atlantic subsurface temperatures: response to a shutdown of the overturning circulation and consequences for its recovery. J. Clim. 20, 4884–4898. https://doi.org/10.1175/JCLI4280.1.

Mudelsee, M., 2014. Climate Time Series Analysis, Atmospheric and Oceanographic Sciences Library. Springer International Publishing, Cham. https://doi.org/10.1007/978-3-319-04450-7.

Mulitza, S., Chiessi, C.M., Schefuß, E., Lippold, J., Wichmann, D., Antz, B., Mackensen, A., Paul, A., Prange, M., Rehfeld, K., Werner, M., Bickert, T., Frank, N., Kuhnert, H., Lynch-Stieglitz, J., Portilho-Ramos, R.C., Sawakuchi, A.O., Schulz, M., Schwenk, T., Tiedemann, R., Vahlenkamp, M., Zhang, Y., 2017. Synchronous and proportional deglacial changes in Atlantic meridional overturning and northeast Brazilian precipitation. Paleoceanography. https://doi.org/10.1002/2017PA003084.

NGRIP Community Members, 2004. High-resolution record of Northern Hemisphere climate extending into the last interglacial period. Nature 431, 147–151. https://doi.org/10.1038/nature02805.

Pedro, J.B., Jochum, M., Buizert, C., He, F., Barker, S., Rasmussen, S.O., 2018. Beyond the bipolar seesaw: toward a process understanding of interhemispheric coupling. Quat. Sci. Rev. 192, 27–46. https://doi.org/10.1016/j.quascirev.2018.05.005.

Peltier, W.R., Vettoretti, G., 2014. Dansgaard-Oeschger oscillations predicted in a comprehensive model of glacial climate: a "kicked" salt oscillator in the Atlantic. Geophys. Res. Lett. 41, 7306–7313. https://doi.org/10.1002/

2014GL061413.

Polanco-martínez, J.M., Medina-elizalde, M.A., Fernanda, M., Goñi, S., 2019. BIN-COR : an R package to estimate the correlation between two unevenly spaced time series. R J 1–14. https://doi.org/10.32614/RJ-2019-035.

Rahmstorf, S., Crucifix, M., Ganopolski, A., Goosse, H., Kamenkovich, I., Knutti, R., Lohmann, G., Marsh, R., Mysak, L.A., Wang, Z., Weaver, A.J., 2005. Thermohaline circulation hysteresis: a model intercomparison. Geophys. Res. Lett. 32, L23605. https://doi.org/10.1029/2005GL023655.

Rasmussen, T.L., Thomsen, E., Moros, M., 2016. North Atlantic warming during Dansgaard-Oeschger events synchronous with Antarctic warming and out-of-phase with Greenland climate. Sci. Rep. 6, 20535. https://doi.org/10.1038/srep20535.

Regenberg, M., Steph, S., Nürnberg, D., Tiedemann, R., Garbe-Schönberg, D., 2009. Calibrating Mg/Ca ratios of multiple planktonic foraminiferal species with δ^{18}O-calcification temperatures: paleothermometry for the upper water column. Earth Planet Sci. Lett. 278, 324–336. https://doi.org/10.1016/j.epsl.2008.12.019.

Reimer, P.J., Bard, E., Bayliss, A., Beck, J.W., Blackwell, P.G., Ramsey, C.B., 2013. IntCal13 and Marine13 radiocarbon age calibration curves 0–50,000 Years cal BP. Radiocarbon 55, 1869–1887. https://doi.org/10.2458/azu_js_rc.55.16947.

Richardson, P.L., 2007. Agulhas leakage into the Atlantic estimated with subsurface floats and surface drifters. Deep. Res. Part I Oceanogr. Res. Pap. 54, 1361–1389. https://doi.org/10.1016/j.dsr.2007.04.010.

Rühlemann, C., Mulitza, S., Lohmann, G., Paul, A., Prange, M., Wefer, G., 2004. Intermediate depth warming in the tropical Atlantic related to weakened thermohaline circulation: combining paleoclimate data and modeling results for the last deglaciation. Paleoceanography 19. https://doi.org/10.1029/2003PA000948.

Sakai, K., Peltier, W.R., 1999. A dynamical systems model of the dansgaard–oeschger oscillation and the origin of the bond cycle. J. Clim. 12, 2238–2255. https://doi.org/10.1175/1520-0442(1999)012<2238:ADSMOT>2.0.CO;2.

Santos, T.P., Lessa, D.O., Venancio, I.M., Chiessi, C.M., Mulitza, S., Kuhnert, H., Govin, A., Machado, T., Costa, K.B., Toledo, F., Dias, B.B., Albuquerque, A.L.S., 2017a. Prolonged warming of the Brazil Current precedes deglaciations. Earth Planet Sci. Lett. 463, 1–12. https://doi.org/10.1016/j.epsl.2017.01.014.

Santos, T.P., Lessa, D.O., Venancio, I.M., Chiessi, C.M., Mulitza, S., Kuhnert, H., Albuquerque, A.L.S., 2017b. The impact of the AMOC resumption in the western South Atlantic thermocline at the onset of the Last Interglacial. Geophys. Res. Lett. https://doi.org/10.1002/2017GL074457.

Schlitzer, R., 2017. Ocean Data View. odv.awi.de.

Schmidt, M.W., Chang, P., Hertzberg, J.E., Them, T.R., Ji, L., Otto-Bliesner, B.L., 2012. Impact of abrupt deglacial climate change on tropical Atlantic subsurface temperatures. Proc. Natl. Acad. Sci. Unit. States Am. 109, 14348–14352. https://doi.org/10.1073/pnas.1207806109.

Schmittner, A., Saenko, O.A., Weaver, A.J., 2003. Coupling of the hemispheres in observations and simulations of glacial climate change. Quat. Sci. Rev. 22, 659–671. https://doi.org/10.1016/S0277-3791(02)00184-1.

Seidov, D., Maslin, M., 2001. Atlantic Ocean heat piracy and the bipolar climate seesaw during Heinrich and Dansgaard-Oeschger events. J. Quat. Sci. 16, 321–328. https://doi.org/10.1002/jqs.595.

Shackleton, N.J., 1974. Attainment of isotopic equilibrium between ocean water and the benthonic foraminifera geuns Uvigerina: isotopic changes in the ocean during the last glacial. Colloq. Int. du C.N.R.S. 219, 203–210.

Shackleton, N.J., Hall, M.A., Vincent, E., 2000. Phase relationships between millennial-scale events 64,000- 24,000 years ago. Paleoceanography 15, 565–569.

Skinner, L.C., Elderfield, H., 2007. Rapid fluctuations in the deep North Atlantic heat budget during the last glacial period. Paleoceanography 22, 1–9. https://doi.org/10.1029/2006PA001338.

Steig, E.J., Alley, R.B., 2002. Phase relationship between Antarctic and Greenland climate records. Ann. Glaciol. 35, 451–456.

Steinke, S., Groeneveld, J., Johnstone, H., Rendle-Bühring, R., 2010. East Asian summer monsoon weakening after 7.5Ma: evidence from combined planktonic foraminifera Mg/Ca and δ^{18}O (ODP Site 1146; northern South China Sea). Palaeogeogr. Palaeoclimatol. Palaeoecol. 289, 33–43. https://doi.org/10.1016/j.palaeo.2010.02.007.

Stocker, T.F., Johnsen, S.J., 2003. A minimum thermodynamic model for the bipolar seesaw. Paleoceanography 18. https://doi.org/10.1029/2003PA000920.

Stramma, L., England, M., 1999. On the water masses and mean circulation of the South Atlantic Ocean. J. Geophys. Res. Ocean. 104, 20863–20883. https://doi.org/10.1029/1999JC900139.

Thornalley, D.J.R., Barker, S., Becker, J., Hall, I.R., Knorr, G., 2013. Abrupt changes in deep Atlantic circulation during the transition to full glacial conditions. Paleoceanography 28, 253–262. https://doi.org/10.1002/palo.20025.

Vázquez Riveiros, N., Govin, A., Waelbroeck, C., Mackensen, A., Michel, E., Moreira, S., Bouinot, T., Caillon, N., Orgun, A., Brandon, M., 2016. Mg/Ca thermometry in planktic foraminifera: improving paleotemperature estimations for G. bulloides and N. pachyderma left. Geochemistry, Geophys. Geosystems 17, 1249–1264. https://doi.org/10.1002/2015GC006234.

Venancio, I.M., Belem, A.L., dos Santos, T.H.R., Zucchi, M. do R., Azevedo, A.E.G., Capilla, R., Albuquerque, A.L.S., 2014. Influence of continental shelf processes in the water mass balance and productivity from stable isotope data on the Southeastern Brazilian coast. J. Mar. Syst. 139, 241–247. https://doi.org/10.1016/j.jmarsys.2014.06.009.

Venancio, I.M., Mulitza, S., Govin, A., Santos, T.P., Lessa, D.O., Albuquerque, A.L.S., Chiessi, C.M., Tiedemann, R., Vahlenkamp, M., Bickert, T., Schulz, M., 2018. Millennial- to orbital-scale responses of western equatorial atlantic thermocline depth to changes in the trade wind system since the last interglacial. Paleoceanogr. Paleoclimatol. 33, 1490–1507. https://doi.org/10.1029/2018PA003437.

Veres, D., Bazin, L., Landais, a., Toyé Mahamadou Kele, H., Lemieux-Dudon, B., Parrenin, F., Martinerie, P., Blayo, E., Blunier, T., Capron, E., Chappellaz, J., Rasmussen, S.O., Severi, M., Svensson, a., Vinther, B., Wolff, E.W., 2013. The Antarctic ice core chronology (AICC2012): an optimized multi-parameter and multi-site dating approach for the last 120 thousand years. Clim. Past 9, 1733–1748. https://doi.org/10.5194/cp-9-1733-2013.

Vettoretti, G., Peltier, W.R., 2015. Interhemispheric air temperature phase relationships in the nonlinear Dansgaard-Oeschger oscillation 1180–1189. https://doi.org/10.1002/2014GL062898.

Voelker, A.H.L., 2002. Global distribution of centennial-scale records for Marine Isotope Stage (MIS) 3: a database. Quat. Sci. Rev. 21, 1185–1212. https://doi.org/10.1016/S0277-3791(01)00139-1.

Wais Divede Project Members, 2013. Onset of deglacial warming in West Antarctica driven by local orbital forcing. Nature 500, 440–444. https://doi.org/10.1038/nature12376.

WAIS Divide Project Members, 2015. Precise interpolar phasing of abrupt climate change during the last ice age. Nature 520, 661–665. https://doi.org/10.1038/nature14401.

Wang, Y., Cheng, H., Edwards, R.L., Kong, X., Shao, X., Chen, S., Wu, J., Jiang, X., Wang, X., An, Z., 2008. Millennial- and orbital-scale changes in the East Asian monsoon over the past 224,000 years. Nature 451, 1090–1093. https://doi.org/10.1038/nature06692.

Weldeab, S., Schneider, R.R., Kölling, M., 2006. Comparison of foraminiferal cleaning procedures for Mg/Ca paleothermometry on core material deposited under varying terrigenous-input and bottom water conditions. Geochemistry, Geophys. Geosystems 7. https://doi.org/10.1029/2005GC000990 n/a-n/a.

Zarriess, M., Johnstone, H., Prange, M., Steph, S., Groeneveld, J., Mulitza, S., MacKensen, A., 2011. Bipolar seesaw in the northeastern tropical Atlantic during Heinrich stadials. Geophys. Res. Lett. 38, 3–8. https://doi.org/10.1029/2010GL046070.

Zhang, X., Lohmann, G., Knorr, G., Purcell, C., 2014. Abrupt glacial climate shifts controlled by ice sheet changes. Nature. https://doi.org/10.1038/nature13592.